Journal of Medicinal Chemistry

Article

pubs.acs.org/jmc

Discovery and Structure-Guided Optimization of Diarylmethanesulfonamide Disrupters of Glucokinase–Glucokinase Regulatory Protein (GK–GKRP) Binding: Strategic Use of a N → S ($n_N \rightarrow \sigma^*_{S-X}$) Interaction for Conformational Constraint

Lewis D. Pennington,[*,†,#] Michael D. Bartberger,[*,‡] Michael D. Croghan,[†] Kristin L. Andrews,[‡] Kate S. Ashton,[†] Matthew P. Bourbeau,[†] Jie Chen,[§] Samer Chmait,[‡] Rod Cupples,[∥] Christopher Fotsch,[†] Joan Helmering,[∥] Fang-Tsao Hong,[†] Randall W. Hungate,[†] Steven R. Jordan,[‡] Ke Kong,[†] Longbin Liu,[†] Klaus Michelsen,[‡] Carolyn Moyer,[⊥] Nobuko Nishimura,[†] Mark H. Norman,[†] Andreas Reichelt,[†] Aaron C. Siegmund,[†] Glenn Sivits,[∥] Seifu Tadesse,[†] Christopher M. Tegley,[†] Gwyneth Van,[⊥] Kevin C. Yang,[†] Guomin Yao,[†] Jiandong Zhang,[‡] David J. Lloyd,[∥] Clarence Hale,[∥] and David J. St. Jean, Jr.[†]

[†]Medicinal Chemistry, [‡]Molecular Structure and Characterization, [§]Pharmacokinetics and Drug Metabolism, [∥]Metabolic Disorders Research, and [⊥]Pathology, Amgen, One Amgen Center Drive, Thousand Oaks, California 91320-1799, United States

Supporting Information

ABSTRACT: The HTS-based discovery and structure-guided optimization of a novel series of GKRP-selective GK–GKRP disrupters are revealed. Diarylmethanesulfonamide hit **6** (hGK–hGKRP IC_{50} = 1.2 μM) was optimized to lead compound **32** (AMG-0696; hGK–hGKRP IC_{50} = 0.0038 μM). A stabilizing interaction between a nitrogen atom lone pair and an aromatic sulfur system ($n_N \rightarrow \sigma^*_{S-X}$) in **32** was exploited to conformationally constrain a biaryl linkage and allow contact with key residues in GKRP. Lead compound **32** was shown to induce GK translocation from the nucleus to the cytoplasm in rats (IHC score = 0; 10 mg/kg po, 6 h) and blood glucose reduction in mice (POC = −45%; 100 mg/kg po, 3 h). X-ray analyses of **32** and several precursors bound to GKRP were also obtained. This novel disrupter of GK–GKRP binding enables further exploration of GKRP as a potential therapeutic target for type II diabetes and highlights the value of exploiting unconventional nonbonded interactions in drug design.

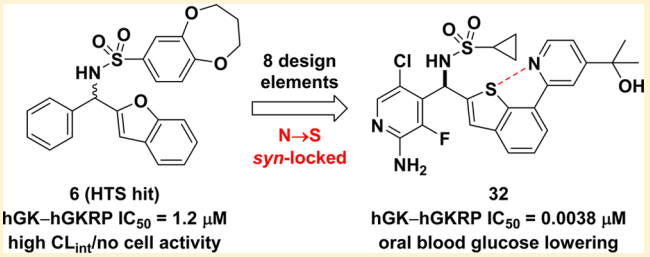

INTRODUCTION

Type II diabetes mellitus (T2DM) is a grievous glucose utilization disorder afflicting nearly 400 million individuals globally at an annual cost of almost 500 billion dollars.[1] In coming decades, aging populations in advanced countries and expanding middle classes in developing nations are expected to increase the number of obese and sedentary people at most risk of suffering this progressively debilitating disease.[2] Although many oral therapies for T2DM have been developed over the past 60 years, including agents that stimulate insulin secretion, improve insulin sensitivity, reduce glucose production, or increase glucose excretion by the selective modulation of therapeutic targets in a variety of biological pathways, ultimate recourse to injectable insulin therapy often has remained necessary.[3] Safe and orally bioavailable drugs directed at novel therapeutic targets are needed to improve the management of T2DM.

Glucokinase (GK) plays a key role in glucose homeostasis through its physiological function converting glucose (**1**) to glucose 6-phosphate (**2**, G6P, Figure 1).[4] GK activity in the liver mediates glucose storage and disposal processes, as G6P is the first intermediate in glycogen synthesis and glycolysis, and GK activity in the pancreas modulates insulin secretion.[5] Many allosteric activators of GK have entered clinical development for the treatment of T2DM;[6] however, observations of hypoglycemia due to GK overactivation have complicated the progression of these potential drug candidates.[7] A number of strategies to circumvent this issue are being pursued, such as liver-selective or partial activators of GK.[8] An alternative strategy is to identify agents that alter the amount of physiologically active GK in selected tissues without affecting its intrinsic catalytic activity.

Glucokinase regulatory protein (GKRP) and glucose cooperatively regulate the cellular location and activity of GK in hepatocytes.[9] A high intracellular concentration of glucose

Received: September 4, 2015

DOI: 10.1021/acs.jmedchem.5b01367
J. Med. Chem. XXXX, XXX, XXX–XXX

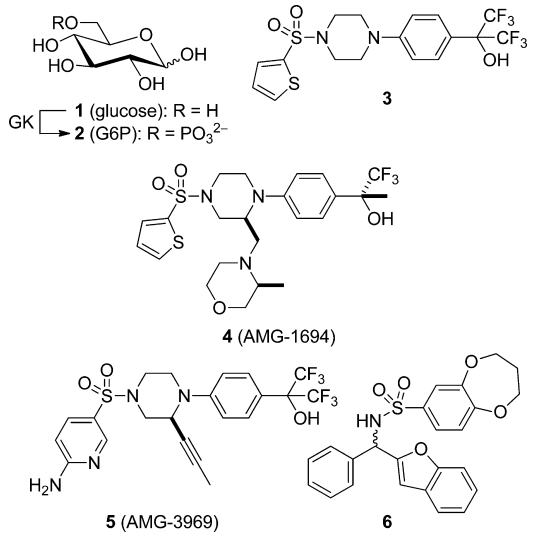

Figure 1. GKRP-selective GK–GKRP disrupters **3**–**6** capable of liberating GK for the conversion of glucose (**1**) to glucose 6-phosphate (G6P; **2**).

(>5.0 mM) disrupts the inactive GK–GKRP complex that is sequestered in the nucleus, allows GK translocation to the cytosol, and stimulates GK activity.[10] Seminal studies of the antidiabetic effects of synthetic ligands that disrupt the GK–GKRP complex by selectively targeting a formerly unknown allosteric binding site on GKRP were recently reported (Figure 1).[11] By use of structure-guided drug design, the original hit **3** (hGK–hGKRP IC_{50} = 1.4 μM) from the first HTS campaign was transformed initially to the first orally active tool compound **4** (AMG-1694; hGK–hGKRP IC_{50} = 0.021 μM)[12] and ultimately to the optimized analogue **5** (AMG-3969; hGK–hGKRP IC_{50} = 0.0037 μM).[13] In db/db mice, a single oral dose (100 mg/kg) of **5** was found to effect nearly complete GK translocation from the nucleus to the cytoplasm (IHC score = 0) with concomitant blood glucose reduction (POC = −60%) at the 6 h time point.[13] To further explore the preclinical pharmacology of this potential therapeutic target for T2DM, structurally distinct GKRP-selective GK–GKRP disrupters were sought.[14]

RESULTS AND DISCUSSION

A second HTS campaign[15] of a separate small-molecule library of over 126 000 compounds identified a single potent and selective hit, *N*-(1-benzofuran-2-yl(phenyl)methyl)-3,4-dihydro-2*H*-1,5-benzodioxepine-7-sulfonamide (**6**, Figure 1).[16] In these luciferase-based luminescence assays measuring ATP depletion, **6** was found to increase GK activity in the presence of GKRP (hGK–hGKRP ATP EC_{50} = 0.26 μM) but to have no effect on GK activity in the absence of GKRP (hGK ATP EC_{50} > 100 μM).[15] Subsequently, HTS hit **6** was demonstrated in surface plasmon resonance assays to selectively bind GKRP (hGKRP K_d = 1.1 μM; hGK K_d > 20 μM) and was shown in a bead-based proximity assay (AlphaScreen) to disrupt the GK–GKRP binding interaction (hGK–hGKRP IC_{50} = 1.2 μM).[17] The favorable biological activity of **6** coupled with its reasonable molecular and physicochemical properties (MW = 435, PSA = 78 Å^2, cLogP = 5.0)[18] encouraged the pursuit of analogues that might exhibit improved pharmacological profiles.

An overlay of the X-ray crystal structures of the original HTS hit **3** and this new HTS hit **6** bound to GKRP is depicted in Figure 2 (2.5 and 2.2 Å resolution, respectively) and highlights the key similarities and differences in the binding modes of

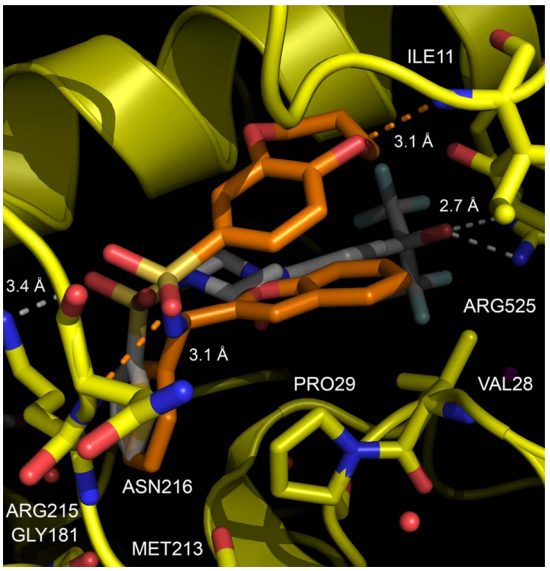

Figure 2. Overlay of the X-ray crystal structures of **3** (transparent white) and **6** (orange) bound to hGKRP (yellow), PDB codes 4MSU and 4PX2, respectively. Hydrogen bonding interactions are represented by dashed lines; residues and interatomic distances (in Å) of note are labeled in white.

these two chemotypes.[12] Notably, **6** was shown to occupy the same allosteric binding site on GKRP as compounds **3**–**5** with negligible differences in protein secondary structure.[11−13,19] During refinement, the *R* enantiomer of racemate **6** was calculated to fit the ligand electron density better than its *S*-configured antipode and to project the sulfonamide NH group away from a hydrophobic pocket and toward bulk solvent. Though the phenyl ring of **6** resides in the same region of the binding pocket as the thiophene ring of **3**, these compounds otherwise have markedly different binding modes. The benzofuran ring system of **6** is shifted over the proline shelf region[14b] compared to the *N*-phenylpiperazine core of **3**, and one of the oxygen atoms of the sulfonamide functionality of **6** engages in an intermolecular hydrogen bond with Asn216 rather than Arg215 as observed for **3**. Furthermore, while **6** does not engage Arg525, one of the oxygen atoms of its benzodioxepine ring system was shown to displace the water molecule present in the X-ray crystal structure of **3**[12] and to form a hydrogen bond with Ile11.

Because the resolution of the X-ray crystal structure depicted in Figure 2 was insufficient for unambiguous assignment of the absolute stereochemistry of the bound and presumably preferred enantiomer of **6**, recourse to chemical synthesis and correlation was made (Scheme 1). First, racemate **6** was resolved using chiral SFC to the proposed *R*-configured eutomer **7** (hGK–hGKRP IC_{50} = 0.87 μM) and the putatively *S*-configured distomer (hGK–hGKRP IC_{50} = 17 μM). Next, the commercially available hydrochloride salt of racemic 1-(1-benzofuran-2-yl)-1-phenylmethanamine (**8**) was free-based (aq $NaHCO_3$) and the resulting neutral amine was resolved using chiral SFC to the known *R*-configured amine **9** and its known *S*-configured antipode,[20] both of which were sulfonylated independently using commercially available 3,4-dihydro-2*H*-1,5-benzodioxepine-7-sulfonyl chloride (**10**) to the correspond-

DOI: 10.1021/acs.jmedchem.5b01367
J. Med. Chem. XXXX, XXX, XXX−XXX

Scheme 1. Determination of the Absolute Stereochemistry of the Eutomer 7

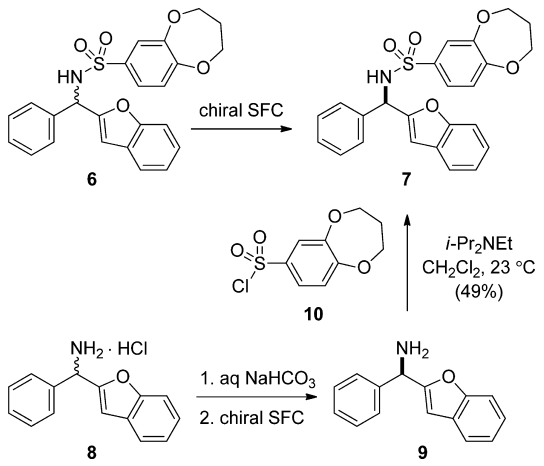

ing *R*- and *S*-configured sulfonamides, respectively. By comparison of chiral HPLC retention times, the eutomer **7** was confirmed to possess the *R* configuration and the distomer was verified to have the *S* absolute stereochemistry.

Though benzodioxepine-based diarylmethanesulfonamide **7** exhibits modest biochemical potency toward disrupting the GK–GKRP binding interaction as reiterated in Table 1 (hGK–hGKRP IC_{50} = 0.87 μM),[17] it does not display measurable cellular potency in an antibody-based assay of GK translocation in mouse hepatocytes (mGK TL EC_{50} > 12.5 μM).[21] Analysis of the X-ray crystal structure depicted in Figure 2 suggested that a substituent at the ortho position of the phenyl ring of the ligand, oriented away from the sulfonamide NH group, could potentially occupy an unfilled niche in the binding site of the protein. Pleasingly, ortho-chloro analogue **11** was found to exhibit significantly improved biochemical and cellular potency (hGK–hGKRP IC_{50} = 0.052 μM; mGK TL EC_{50} = 6.3 μM).[17,21] Further potency enhancement was realized upon replacing the benzofuran ring of **11** with a benzothiophene ring, as in **12** (hGK–hGKRP IC_{50} = 0.017 μM; mGK TL EC_{50} = 2.9 μM). It was also not surprising that **12** was shown to retain selective binding affinity for GKRP (hGKRP K_d = 0.019 μM; hGK K_d > 10 μM).[17]

Disappointingly, compounds **7**, **11**, and **12** all suffer high clearance in rat liver microsomes (RLM CL_{int} > 399 μL min^{-1} mg^{-1}). A preliminary metabolite identification study of **12** using rat liver microsomes indicated that the major metabolite arose from oxidation and cleavage of the methylene chain of the benzodioxepine moiety. Examination of the X-ray crystal structure illustrated in Figure 2 and computational modeling indicated that substitution of the central carbon atom of the methylene chain with either a F atom with the *S* configuration (axial) or an OH group with the *R* configuration (equatorial) might be accommodated in a hydrophobic cleft or hydrophilic pocket of the binding site, respectively. These strategems were quickly tested using the *R*,*S*-hydroxyl- (**13**), *R*,*S*-fluoro- (**14**), and *gem*-difluoro- (**15**) analogues, which led to only moderate biochemical potency loss for **13** and **14** but which resulted in little to no improvement in microsomal stability for any of the compounds (hGK–hGKRP IC_{50} = 0.10, 0.074, and 0.81 μM, respectively; RLM CL_{int} = 304, >399, and >399 μL min^{-1} mg^{-1}, respectively). Attempts to improve the microsomal stability of **12** by inserting N atoms into the scaffold to lower its lipophilicity (cLogP of **12** = 6.2) were also unsuccessful, as illustrated for diaza-analogue **16** (cLogP = 4.0; hGK–hGKRP IC_{50} = 0.16 μM; RLM CL_{int} > 399 μL min^{-1} mg^{-1}).

Since modification of the benzodioxepine moiety of **12** did not appear to be a viable approach to improving microsomal stability, systematic evaluation of the effects of truncating it was undertaken (Table 2). Surprisingly, excising just one or two methylene groups from the seven-membered benzodioxepine ring of **12** to give the six- and five-membered benzodioxine and benzodioxole analogues **17** and **18**, respectively, was found to result in a precipitous loss of biochemical and cellular potency with no gain in microsomal stability (hGK–hGKRP IC_{50} = 2.5

Table 1. Optimization of Benzodioxepine-Based Diarylmethanesulfonamide Disrupters of GK–GKRP Binding

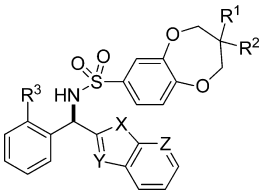

compd	R^1	R^2	R^3	X	Y	Z	hGK–hGKRP IC_{50}[a] (μM)	mGK TL EC_{50}[b] (μM)	RLM CL_{int}[c] (μL min^{-1} mg^{-1})	cLogP[d]
7	H	H	H	O	CH	CH	0.87	>12.5	>399	5.0
11	H	H	Cl	O	CH	CH	0.052	6.3[e]	>399	5.7
12	H	H	Cl	S	CH	CH	0.017	2.9	>399	6.2
13	H	OH[f]	Cl	S	CH	CH	0.10	4.3	304	5.1
14	H	F[f]	Cl	S	CH	CH	0.074	4.1	>399	6.5
15	F	F	Cl	S	CH	CH	0.81[e]	>12.5	>399	7.4
16	H	H	Cl	S	N	N	0.16	3.3	>399	4.0

[a]Inhibition of the GK–GKRP binding interaction as measured in a bead-based proximity assay (AlphaScreen) using human GK and GKRP constructs. Data represent an average of at least three measurements unless otherwise indicated. Standard deviations are reported in the Supporting Information. [b]GK translocation (TL) as measured in an antibody-based assay using mouse hepatocytes. Data represent an average of at least 3 measurements unless otherwise indicated (for EC_{50} > 12.5 μM, data represent 1 measurement). Standard deviations are reported in the Supporting Information. [c]Estimated intrinsic clearance (CL_{int}) determined by incubation of test compound with rat liver microsomes (RLM) at 37 °C for 30 min and measurement of percent turnover. [d]Calculated using Daylight Chemical Information Systems software (Web site: www.daylight.com). [e]Data represent an average of two measurements. Standard deviations are reported in the Supporting Information. [f]Prepared and tested as a 1:1 mixture of epimers at this stereocenter.

DOI: 10.1021/acs.jmedchem.5b01367
J. Med. Chem. XXXX, XXX, XXX–XXX

Table 2. Systematic Truncation of the Benzodioxepine Moiety

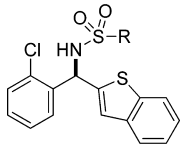

compd	R	hGK–hGKRP IC_{50}[a] (μM)	mGK TL EC_{50}[b] (μM)	RLM CL_{int}[c] (μL min^{-1} mg^{-1})
12		0.017	2.9	>399
17		2.5	>12.5	>399
18		6.5	>12.5	>399
19		7.3	>12.5	>399
20		>33	>12.5	>399
21		>33	>12.5	>399

[a]Inhibition of the GK–GKRP binding interaction as measured in a bead-based proximity assay (AlphaScreen) using human GK and GKRP constructs. Data represent an average of at least three measurements (for EC_{50} > 33 μM, data represent two measurements). Standard deviations are reported in the Supporting Information. [b]GK translocation (TL) as measured in an antibody-based assay using mouse hepatocytes. Data represent an average of at least three measurements (for EC_{50} > 12.5 μM, data represent one measurement). Standard deviations are reported in the Supporting Information. [c]Estimated intrinsic clearance (CL_{int}) determined by incubation of test compound with rat liver microsomes (RLM) at 37 °C for 30 min and measurement of percent turnover.

and 6.5 μM, respectively; mGK TL EC_{50} > 12.5 μM and RLM CL_{int} > 399 μL min^{-1} mg^{-1} for both **17** and **18**). The para-methoxyphenyl-, phenyl-, and cyclopropyl analogues **19**–**21** were also shown to exhibit poor biochemical and cellular potency and high microsomal turnover (hGK–hGKRP IC_{50} = 7.3, >33, and >33 μM, respectively; mGK TL EC_{50} > 12.5 μM and RLM CL_{int} > 399 μL min^{-1} mg^{-1} for **19**–**21**). Because replacement of the microsomally labile benzodioxepine moiety of **12** did not lead to improved stability for **17**–**21**, it was speculated that the site of metabolism had shifted to another part of the scaffold in these truncated analogues. At this juncture, reassessment of the lead optimization direction was necessary.

A top-view alignment of the X-ray crystal structures of the biochemically equipotent **4** and benzodioxepine **12** bound to GKRP is shown in Figure 3 (2.4 Å resolution for both **4** and **12**; hGK–hGKRP IC_{50} = 0.021 and 0.017 μM for **4** and **12**, respectively).[12] As previously noted for HTS hits **3** and **6**, the sulfonyl groups of **4** and **12** interact with different residues (Arg215 and Asn216, respectively). In contrast, it was observed that the benzodioxepine oxygen atom of **12** para to the sulfonamide group is nearly superimposable with the oxygen atom of the morpholine ring of **4** and that both of them engage in intermolecular hydrogen bonds with Ile11.[12] It is also

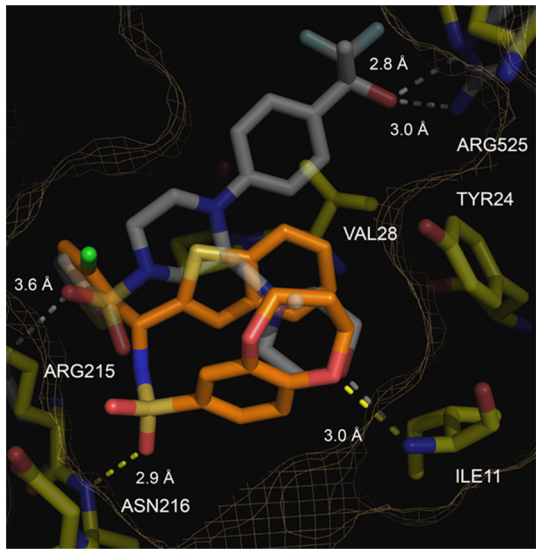

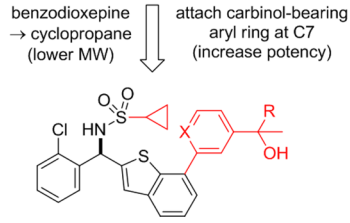

Figure 3. Top-view overlay of the X-ray crystal structures of **4** (transparent white) and **12** (orange) bound to hGKRP (yellow), PDB codes 4LY9 and 4PX3, respectively. Hydrogen bonding interactions are represented by dashed lines; residues and interatomic distances (in Å) of note are labeled in white. Schematic depicts resultant proposed structure modifications.

interesting to note that, as with the benzodioxepine moiety of **12**, the morpholine ring of **4** was found to be microsomally labile,[12] requiring replacement with a propynyl group during the lead optimization effort culminating in the identification of microsomally stable **5**.[13]

The upper portion of Figure 3 also illustrates the bifurcated hydrogen bonding interaction between the carbinol group of **4** and the guanidinium side chain of Arg525.[12] Notably, an Arg525-engaging substituent, whether a carbinol or a suitable replacement, has served as a potency mainstay in all GKRP disrupters reported to date.[11−14] In contrast, this region of the GKRP binding site is completely unoccupied in the binding mode of **12**. It was therefore proposed that introduction of an Arg525-engaging moiety onto C7 of the benzothiophene ring of **12** might improve its potency and allow truncation of the bulky and microsomally labile benzodioxepine ring system. Due to the steric constraints imposed by the constricted nature of the Arg525 region of the GKRP binding site, it was clear that access to this residue would require a nearly coplanar arrangement of the benzothiophene moiety and the ring bearing the guanidine-engaging substituent. Given the preference for ≥45° dihedral angles in biphenyl systems,[22] the use of a C7-phenyl ring to bear the 4′-carbinol moiety (Figure 3; X = CH) was not expected to be optimal.

Intramolecular interactions of sulfur atoms in aromatic systems with O and N donor atoms (e.g., O → S and N → S) have been the subject of significant attention in the theoretical, spectroscopic, and crystallographic literature but have not been exploited to a significant extent in drug discovery

DOI: 10.1021/acs.jmedchem.5b01367
J. Med. Chem. XXXX, XXX, XXX−XXX

efforts.[23] For systems possessing an aromatic sulfur atom and a nearby heteroatom bearing a lone pair (e.g., carbonyl group, heteroaromatic ring, etc.) with a favorable orientation with respect to sulfur, the *syn* conformation is stabilized and, in fact, often dominant. This phenomenon has been ascribed to a stabilizing interaction between the donor lone pair and the σ^* orbital of sulfur and the atom to which it is bonded ($n_{donor} \rightarrow \sigma^*_{S-X}$), outweighing the repulsive interactions between the sulfur and heteroatom lone pairs. Such a "*syn*-locked" effect has been found to be operative in a series of ΔF508-CFTR correctors for the treatment of cystic fibrosis[24] and has been exploited in a recent lead optimization campaign targeting inhibitors of p38α.[25]

Density functional theory calculations,[26] along with natural bond orbital (NBO) analysis of Weinhold,[27,28] demonstrated that a 2-pyridyl substituent attached to C7 of a benzothiophene core (Figure 3; X = N) would exhibit a strong coplanarizing effect due to a nearly geometrically ideal interaction trajectory ($\angle$N−S−C ≈ 168°) between the lone pair of the pyridine nitrogen and the σ^* orbital of the S−C bond (Figure 4). In the context of these benzothiophene-containing GKRP disrupters, this system was predicted to present the C7 pyridyl ring and its accompanying 4′-carbinol functionality in nearly optimal alignment for contact with the distal guanidinium side chain of Arg525. To dramatically lower the molecular weight of the proposed GK−GKRP disrupters bearing a 4′-substituted C7 pyridyl moiety, truncation of the high molecular weight benzodioxepine ring system to the low molecular weight, and presumably more microsomally stable, cyclopropane ring was chosen (Figure 3). Although cyclopropane analogue **21** had been found to suffer high microsomal turnover, it was unclear what effect 2-pyridyl moieties attached to C7 of the benzothiophene core would have on the metabolic stability of the proposed analogues.

The realization of this unconventional design strategy is detailed in Table 3. Compared to the 7-hydridobenzothiophene **21** (hGK−hGKRP IC_{50} > 33 μM), the 7-phenylbenzothiophene analogues **22** and **23** were found to display improved potency toward disrupting the GK−GKRP binding interaction (hGK−hGKRP IC_{50} = 4.4 and 2.7 μM, respectively). Even more strikingly, and as predicted, the 7-pyridylbenzothiophene analogues **24** and **25** were shown to exhibit a further 10-fold improvement in biochemical potency (hGK−hGKRP IC_{50} = 0.30 and 0.19 μM, respectively). These considerable functional activity improvements for 7-pyridylbenzothiophene analogues **24** and **25** are likely driven by their greater GKRP binding affinities as measured in surface plasmon resonance assays (hGKRP K_d = 34, 36, 0.50, and 0.25 μM for **22**−**25**, respectively), a result of a decreased conformational energy penalty required for binding. Pleasingly, compounds **24** and **25** also display low clearance in rat liver microsomes (RLM CL_{int} < 14 μL min^{-1} mg^{-1}).

Unfortunately, **24** and **25** do not exhibit measurable cell potency in mouse hepatocytes (mGK TL EC_{50} > 12.5 μM). As the binding affinities of **24** and **25** to human and mouse GKRP were found to be similar (mGKRP K_d = 1.8 and 0.85 μM, respectively), the low cell potency of **24** and **25** was attributed to their high lipophilicity (cLogP = 5.1; ACDLogP = 6.3; $ACDLogD_{7.4}$ = 6.2) and poor cellular permeability (P_{app} < 1.8 × 10^{-6} cm/s and P_{app} = 2.4 × 10^{-6} cm/s, respectively). The *gem*-dimethylcarbinol analogue **26** was designed to simultaneously decrease lipophilicity and molecular weight, with the added benefit of removing a stereocenter. It is notable that a

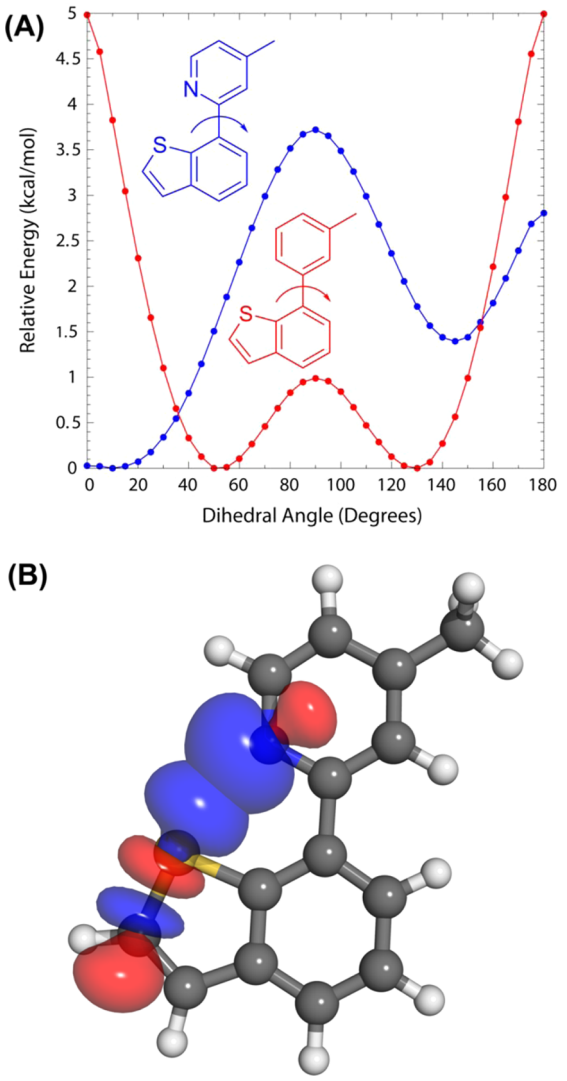

Figure 4. (A) B3LYP/6-31+G(d,p) dihedral plot of model 7-(5′-methyl-2′-pyridyl)benzothiophene and 7-(3′-toluyl)benzothiophene, demonstrating strong *syn*-coplanarizing effect of the N → S interaction. (B) Depiction of the stabilizing interaction between the occupied nitrogen lone pair (n_N) and unoccupied S−C2 (σ^*_{S-C}) NBOs, utilizing the B3LYP/6-31+G(d,p) density.

gem-dimethylcarbinol moiety is not chemically stable in the original *N*-phenylpiperazine series of GKRP disrupters **3**−**5**,[11−13] as this group is para to the amine functionality in these compounds. Gratifyingly, despite displaying similar biochemical potency (hGK−hGKRP IC_{50} = 0.11 μM), the *gem*-dimethylcarbinol analogue **26** was found to exhibit improved cellular permeability and potency (P_{app} = 7.5 × 10^{-6} cm/s; mGK TL EC_{50} = 7.7 μM), with only a slight loss in microsomal stability (RLM CL_{int} = 34 μL min^{-1} mg^{-1}). However, further improvement in biochemical and cellular potency was desired.

A front-view alignment of the X-ray crystal structures of **5** and **26** bound to GKRP is depicted in Figure 5 (2.0 and 2.6 Å resolution, respectively).[13] The crystal structure of **26** with GKRP clearly reveals the *syn*-locked orientation of the benzothiophene sulfur and pyridine nitrogen atoms, as well as the resultant successful engagement of the 4′-*gem*-dimethylcarbinol moiety with the guanidinium side chain of Arg525. Analysis of the 2-chlorophenyl ring of **26** suggested that a F atom at the second ortho position might be

DOI: 10.1021/acs.jmedchem.5b01367
J. Med. Chem. XXXX, XXX, XXX−XXX

Table 3. Modification of the C7 Aryl Ring of Cyclopropane-Based Diarylmethanesulfonamide Disrupters of GK−GKRP Binding

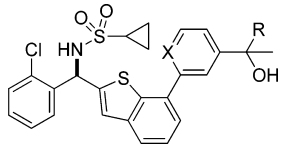

compd	R	X	hGK−hGKRP IC_{50}[a] (μM)	h,r,mGKRP K_d[b] (nM)	mGK TL EC_{50}[c] (μM)	P_{app} (ER)[d] ($\times 10^{-6}$ cm/s)	RLM CL_{int}[e] (μL min^{-1} mg^{-1})	cLogP[f]	ACDLogP (ACDLogD$_{7.4}$)[g]
21[h]			>33	ND[i]	>12.5	ND[i]	>399	4.5	5.7 (5.7)
22	(*R*)-CF_3	CH	4.4	34000[j]	>12.5	ND[i]	<14	6.4	7.6 (7.6)
23	(*S*)-CF_3	CH	2.7	36000[j]	>12.5	ND[i]	<14	6.4	7.6 (7.6)
24	(*R*)-CF_3	N	0.30	500, 430, 1800	>12.5	<1.8 (>2.6)	<14	5.1	6.3 (6.2)
25	(*S*)-CF_3	N	0.19	250, 800, 850	>12.5	2.4 (2.7)	<14	5.1	6.3 (6.2)
26	CH_3	N	0.11	90, 130, 290	7.7	7.5 (2.2)	34	4.8	5.6 (5.6)

[a]Inhibition of the GK−GKRP binding interaction as measured in a bead-based proximity assay (AlphaScreen) using human GK and GKRP constructs. Data represent an average of at least three measurements (for EC_{50} > 33 μM, data represent two measurements). Standard deviations are reported in the Supporting Information. [b]Dissociation constant (K_d) as measured in a surface plasmon resonance assay (Biacore) using human, rat, or mouse GKRP constructs, respectively. Data represent an average of two measurements unless otherwise indicated. Standard deviations are reported in the Supporting Information. [c]GK translocation (TL) as measured in an antibody-based assay using mouse hepatocytes. Data represent an average of at least three measurements (for EC_{50} > 12.5 μM, data represent at least one measurement). Standard deviations are reported in the Supporting Information. [d]Apparent permeability (P_{app} A → B) through porcine proximal tubule cells (LLC-PK1 cell line) and efflux ratio (ER). [e]Estimated intrinsic clearance (CL_{int}) determined by incubation of test compound with rat liver microsomes (RLM) at 37 °C for 30 min and measurement of percent turnover. [f]Calculated using Daylight Chemical Information Systems software (Web site: www.daylight.com). [g]Calculated using Advanced Chemistry Development (ACD/Labs) software (Web site: www.acdlabs.com). [h]Compound **21** only bears an H atom at C7 of the benzothiophene ring system and is included in Table 3 to facilitate comparison with C7-substituted analogues; see Table 2. [i]Not determined (ND). [j]Dissociation constant (K_d) as measured in a surface plasmon resonance assay (Biacore) using human GKRP constructs only. Data represent one measurement.

accommodated and engage in a favorable electrostatic interaction with the sulfonamide NH group (Figure 5; X = CF),[29] which could partially mask this hydrogen bond donor, improve cell permeability, and potentially favor the binding conformation. The alignment of the X-ray crystal structures of **5** and **26** bound to GKRP clearly shows that the potency-enhancing, and lipophilicity-lowering, aminopyridine functionality present in **5** could be incorporated into **26** in an analogous fashion, albeit with differing regiochemistry required for optimal engagement of Gly181 and Met213 (Figure 5; X or Y = CH or N; R = NH_2).

The results of incorporating these design elements are summarized in Table 4. Compared to **26**, ortho-fluoro analogue **27** was found to display 2- to 3-fold better binding affinity (h,r,mGKRP K_d = 0.030, 0.060, and 0.12 μM, respectively) but only marginally improved biochemical potency (hGK−hGKRP IC_{50} = 0.056 μM), cell permeability and potency (P_{app} = 9.5 × 10^{-6} cm/s; mGK TL EC_{50} = 5.2 μM), and microsomal stability (RLM CL_{int} = 18 μL min^{-1} mg^{-1}). In contrast, aminopyridine analogue **28** was shown to exhibit 10- to 20-fold better binding affinity (h,r,mGKRP K_d = 0.0042, 0.013, and 0.024 μM, respectively) and functional activity (hGK−hGKRP IC_{50} = 0.0060 μM; mGK TL EC_{50} = 0.43 μM), as well as slightly improved cellular permeability (P_{app} = 11 × 10^{-6} cm/s), but at the expense of higher microsomal clearance (RLM CL_{int} = 130 μL min^{-1} mg^{-1}) versus **26**. A metabolite identification study of **28** using human liver microsomes revealed that the primary product of metabolism was hydroxylation at the position ortho to the amino group of the aminopyridine ring. Substitution of this site with a F atom gave analogue **29**,[30] which was found to possess significantly improved microsomal clearance (RLM CL_{int} = 28 μL min^{-1} mg^{-1}) and comparable biochemical activity (h,r,mGKRP K_d = 0.0066, 0.017, and 0.035 μM, respectively; hGK−hGKRP IC_{50} = 0.011 μM) but to have nearly 5-fold lower cellular potency (mGK TL EC_{50} = 1.9 μM), despite having similar cellular permeability (P_{app} = 7.8 × 10^{-6} cm/s). Compared to aminopyridine **28**, aminopyridine regioisomer **30** was shown to possess a 2- to 4-fold decrease in binding affinity (h,r,mGKRP K_d = 0.019, 0.013, and 0.052 μM, respectively) and biochemical potency (hGK−hGKRP IC_{50} = 0.025 μM); however, it was found to have improved microsomal stability (RLM CL_{int} = 67 μL min^{-1} mg^{-1}) and cellular permeability (P_{app} = 19 × 10^{-6} cm/s), which likely led to its similar cellular potency (mGK TL EC_{50} = 0.41 μM). The aminopyrimidine **31** was designed to simultaneously block a site of metabolism and possess lower lipophilicity. Analogue **31** exhibits excellent binding affinity (h,r,mGKRP K_d = 0.0086, 0.0079, and 0.031 μM, respectively), biochemical potency (hGK−hGKRP IC_{50} = 0.018 μM), and cellular permeability and potency (P_{app} = 19 × 10^{-6} cm/s; mGK TL EC_{50} = 0.48 μM), as well as low intrinsic clearance (RLM CL_{int} = 28 μL min^{-1} mg^{-1}). Finally, ortho-fluoroaminopyridine analogue **32** was found to display the greatest binding affinity (h,r,mGKRP K_d = 0.0015, 0.0012, and 0.0045 μM, respectively) and biochemical potency (hGK−hGKRP IC_{50} = 0.0038 μM), along with excellent cellular permeability and potency (P_{app} = 16 × 10^{-6} cm/s; mGK TL EC_{50} = 0.066 μM) and low intrinsic clearance (RLM CL_{int} = 26 μL min^{-1} mg^{-1}). It was also pleasing that **31** and **32** were found to retain selective binding affinity for GKRP (hGK K_d > 10 μM for both **31** and **32**).

The X-ray crystal structure of **32** bound to GKRP is shown in Figure 6 (2.2 Å resolution). As expected, the interactions of the sulfonamide group with Asn216 and the carbinol moiety with Arg525, as well as the projection of the cyclopropyl functionality and the coplanar arrangement of the benzothiophene core with the C7-pyridyl ring, were all found to be nearly identical to those observed for **26**. It was also gratifying to observe that the aminopyridine functionality of **32** engaged in

DOI: 10.1021/acs.jmedchem.5b01367
J. Med. Chem. XXXX, XXX, XXX−XXX

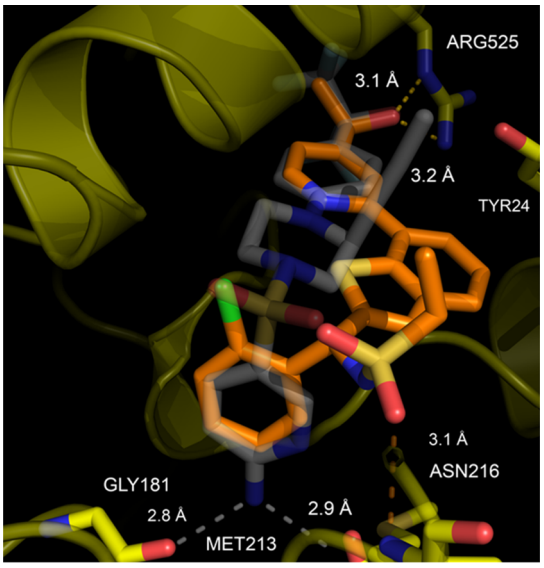

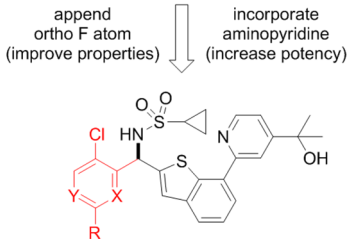

Figure 5. Overlay of the X-ray crystal structures of **5** (transparent white) and **26** (orange) bound to hGKRP (yellow), PDB codes 4MQU and 4PXS, respectively. Hydrogen bonding interactions are represented by dashed lines; residues and interatomic distances (in Å) of note are labeled in white. Schematic depicts resultant proposed structure modifications.

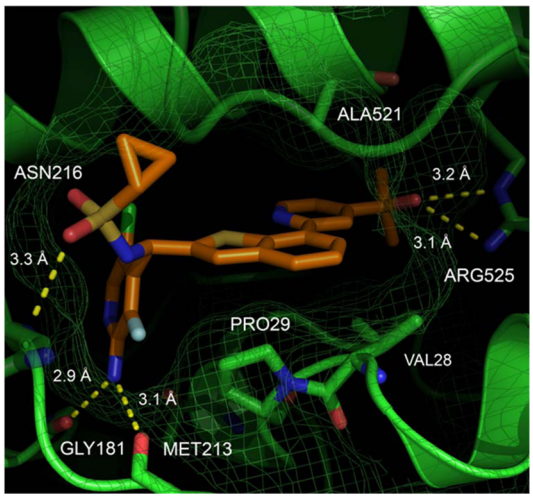

Figure 6. X-ray crystal structure of **32** (orange) bound to hGKRP (green), PDB code 4PX5. Hydrogen bonding interactions are represented by dashed lines, and residues and interatomic distances (in Å) of note are labeled in white.

hydrogen bonds with Gly181 and Met213 as planned. The F atom of the ortho-fluoroaminopyridine moiety of **32**, while possibly affording a small amount of additional van der Waals contact with the solvent-exposed protein surface, also may give rise to a pair of stabilizing electrostatic interactions between both the sulfonamide NH group and one of the H atoms of the pendent NH_2 functionality. This pair of electrostatically favorable interactions could serve to mask and reduce the desolvation penalty of these polar H atoms and stabilize the observed binding orientation of the ring, as well.

Pharmacokinetic profiles were obtained for the two analogues in Table 4 with the best combination of cellular potency and microsomal stability, **31** (AMG-7549) and **32**

Table 4. Modification of the 2-Chlorophenyl Ring of Cyclopropane-Based Diarylmethanesulfonamide Disrupters of GK−GKRP Binding

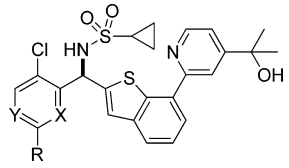

compd	R	X	Y	hGK−hGKRP IC_{50}[a] (μM)	h,r,mGKRP K_d[b] (nM)	mGK TL EC_{50}[c] (μM)	P_{app} (ER)[d] ($\times 10^{-6}$ cm/s)	RLM CL_{int}[e] (μL min^{-1} mg^{-1})	cLogP[f]	ACDLogP (ACDLogD$_{7.4}$)[g]
26	H	CH	CH	0.11	90, 130, 290	7.7	7.5 (2.2)	34	4.8	5.6 (5.6)
27	H	CF	CH	0.056	30, 60, 120	5.2	9.5 (2.3)	18	4.9	5.2 (5.2)
28	NH_2	N	CH	0.0060	4.2, 13, 24	0.43	11 (2.0)	130	3.1	4.5 (4.3)
29	NH_2	N	CF	0.011	6.6, 17, 35	1.9	7.8 (1.8)	28	3.2	4.4 (4.0)
30	NH_2	CH	N	0.025	19, 13, 52	0.41	19 (1.7)	67	3.1	4.5 (4.3)
31	NH_2	N	N	0.018	8.6, 7.9, 31	0.48	19 (2.3)	28	2.3	3.4 (3.2)
32	NH_2	CF	N	0.0038	1.5, 1.2, 4.5	0.066	16 (2.3)	26	3.2	4.4 (3.9)

[a]Inhibition of the GK−GKRP binding interaction as measured in a bead-based proximity assay (AlphaScreen) using human GK and GKRP constructs. Data represent an average of at least three measurements. Standard deviations are reported in the Supporting Information. [b]Dissociation constant (K_d) as measured in a surface plasmon resonance assay (Biacore) using human, rat, or mouse GKRP constructs, respectively. Data represent an average of two measurements. Standard deviations are reported in the Supporting Information. [c]GK translocation (TL) as measured in an antibody-based assay using mouse hepatocytes. Data represent an average of at least three measurements. Standard deviations are reported in the Supporting Information. [d]Apparent permeability (P_{app} A → B) through porcine proximal tubule cells (LLC-PK1 cell line) and efflux ratio (ER). [e]Estimated intrinsic clearance (CL_{int}) determined by incubation of test compound with rat liver microsomes (RLM) at 37 °C for 30 min and measurement of percent turnover. [f]Calculated using Daylight Chemical Information Systems software (Web site: www.daylight.com). [g]Calculated using Advanced Chemistry Development (ACD/Labs) software (Web site: www.acdlabs.com).

DOI: 10.1021/acs.jmedchem.5b01367
J. Med. Chem. XXXX, XXX, XXX−XXX

Table 5. Pharmacokinetic Profiles of Key Compounds 31 and 32

compd[a]	PPB (%)[b]	CL (L h^{-1} kg^{-1})[c]	V_{dss} (L/kg)[c]	$t_{1/2}$ (h)[c]	C_{max} (μM)[d]	t_{max} (h)[d]	F[e]
	rat	2 mg/kg, iv	2 mg/kg, iv	2 mg/kg, iv	10 mg/kg, po	10 mg/kg, po	(%)
31	99	0.28	1.3	3.0	1.9	4.7	25
32	99	0.36[f]	1.6[f]	3.1[f]	2.8	3.3	46

[a]In vivo experiments were conducted using male Sprague–Dawley rats (N = 3/group unless otherwise indicated). [b]Percent rat plasma protein binding (PPB) as measured in vitro following rapid equilibrium dialysis. [c]Clearance (CL), volume of distribution (V_{dss}), and half-life ($t_{1/2}$) determined following a single intravenous dose (2.0 mg/kg; vehicle = DMSO). [d]Maximal concentration (C_{max}) and time at maximal concentration (t_{max}) determined following a single oral dose (10 mg/kg; vehicle = 1.0% Tween 80, 2.0% HPMC, 97% H_2O, pH 7.0). [e]Percent bioavailability (F) calculated using $AUC_{0\rightarrow\infty}$ values determined from the 2.0 mg/kg (iv) and 10 mg/kg (po) doses. [f]N = 1.

(AMG-0696), in preparation for more detailed studies in vivo (Table 5). Both analogues were found to exhibit high rat plasma protein binding in an in vitro assay employing rapid equilibrium dialysis (PPB = 99% for both **31** and **32**). In male Sprague–Dawley rats (N = 3 and 1 for **31** and **32**, respectively) given a single intravenous dose (2.0 mg/kg), these compounds were shown to display similarly good pharmacokinetic profiles (CL = 0.28 and 0.36 L h^{-1} kg^{-1}, V_{dss} = 1.3 and 1.6 L/kg, and $t_{1/2}$ = 3.0 and 3.1 h for **31** and **32**, respectively). In constrast, in rats (N = 3 for both **31** and **32**) given a single oral dose (10 mg/kg), aminopyrimidine **31** was found to exhibit lower peak concentration, slower absorption, and less bioavailability compared to ortho-fluoroaminopyridine **32** (C_{max} = 1.9 and 2.8 μM, t_{max} = 4.7 and 3.3 h, and F = 25% and 46% for **31** and **32**, respectively).

Because **31** and **32** were shown to display good pharmacokinetic profiles, the pharmacodynamic effects of each compound were evaluated (Figure 7).[31] Six hours after a single 10 or 100 mg/kg oral dose in Sprague–Dawley rats (N = 6 for both doses), aminopyrimidine **31** was found to exhibit dose-proportional plasma exposure ($[\mathbf{31}]_{plasma}$ = 2.9 and 23 μM for the 10 and 100 mg/kg dose, respectively) and robust GK translocation (Figure 7A; IHC score = 0.33 and 0.0 for the 10 and 100 mg/kg dose, respectively). At the 24 h time point, the plasma exposure and pharmacodynamic response for both the 10 and 100 mg/kg doses of **31** were shown to be significantly diminished ($[\mathbf{31}]_{plasma}$ = 0.20 and 0.21 μM, IHC score = 2.3 and 1.3 for the 10 and 100 mg/kg dose, respectively). The pharmacodynamic response for **32** was found to be more robust and durable, with full GK translocation lasting to the 24 h time point for both the 10 and 100 mg/kg doses (Figure 7B; $[\mathbf{32}]_{plasma}$ = 0.22 and 6.3 μM for the 10 and 100 mg/kg dose, respectively; IHC score = 0.0 for both the 10 and 100 mg/kg doses).[32] This effect on GK translocation in Sprague–Dawley rats is consistent with the GK–GKRP disruption activities of **31** and **32**.[11−14]

The blood glucose lowering efficacy of **31** and **32** in the diabetic db/db mouse model was also investigated (Figure 8).[33] Six hours after a single 10, 30, or 100 mg/kg oral dose, aminopyrimidine **31** was found to exhibit dose-proportional whole-blood exposure ($[\mathbf{31}]_{blood}$ = 1.2, 4.1, and 19 μM for the 10, 30, and 100 mg/kg dose, respectively), with statistically significant blood glucose lowering achieved for the 100 mg/kg dose (Figure 8A; POC = −45%).[34,35] Similar to the rat GK translocation response discussed above, the blood glucose lowering activity for **32** in db/db mice was shown to be better than that observed for **31**, with more robust and statistically significant blood glucose lowering attained for the 100 mg/kg dose at both the 3 and 6 h time points (Figure 8B; $[\mathbf{32}]_{blood}$ = 25 and 21 μM, POC = −45% and −33% for the 3 and 6 h time points, respectively).[36,37] This reduction in blood glucose levels in db/db mice is also consistent with the GK–GKRP disruption activities of **31** and **32**.[11−14]

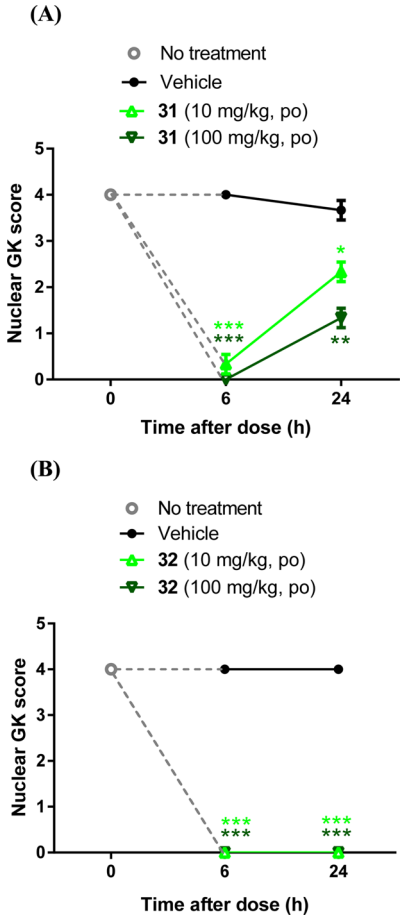

Figure 7. Measurement of GK translocation in Sprague–Dawley rats 6 and 24 h after either a 10 or 100 mg/kg oral dose of (A) **31** or (B) **32**. The statistical significance of the GK translocation measurements was based on comparison to the individual vehicle control groups (N = 6/group; (*) P < 0.05, (**) P < 0.01, and (***) P < 0.001 as calculated by the ANOVA/Dunnett's multiple comparison test).

The synthesis of benzodioxepine-based diarylmethanesulfonamide **12** is described in Scheme 2 and exemplifies the general approach to compounds **12**–**21** in Tables 1 and 2.[38] Commercially available 2-chlorobenzaldehyde (**33**) and (*S*)-2-methyl-2-propanesulfinamide were condensed using $Ti(OEt)_4$ to afford *tert*-butanesulfinylimine **34** in 88% yield. Regioselective deprotonation of commercially available 1-benzothiophene with *n*-butyllithium followed by addition of **34** gave *tert*-butanesulfinamide **35** possessing the *R* absolute stereochemistry at the diarylmethane stereocenter in 65% yield after removal of the minor undesired diastereomer by flash

DOI: 10.1021/acs.jmedchem.5b01367
J. Med. Chem. XXXX, XXX, XXX−XXX

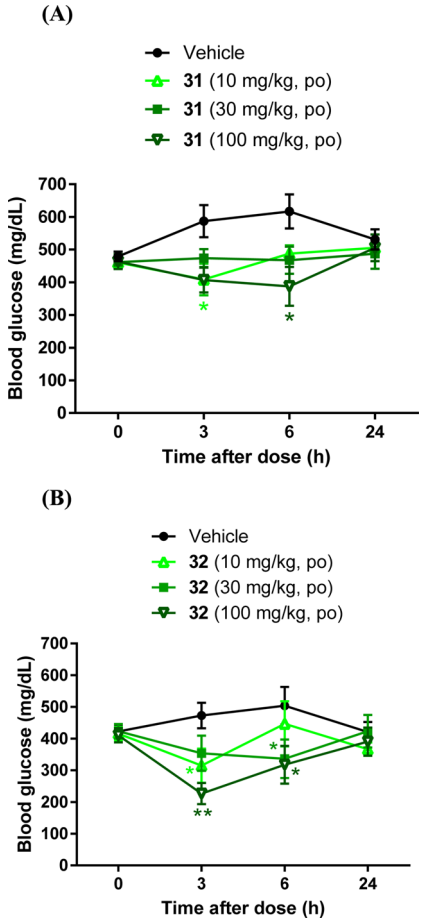

Figure 8. Measurement of blood glucose lowering in db/db mice 3, 6, and 24 h after a 10, 30, or 100 mg/kg oral dose of (A) **31** or (B) **32**. The statistical significance of the blood glucose measurements was based on comparison to the individual vehicle control groups (N = 5–8/group; (*) $P < 0.05$ and (**) $P < 0.01$ as calculated by the ANOVA/Dunnett's multiple comparison test).

Scheme 2. Chemical Synthesis of Benzodioxepine-Based GK–GKRP Disrupter 12[a]

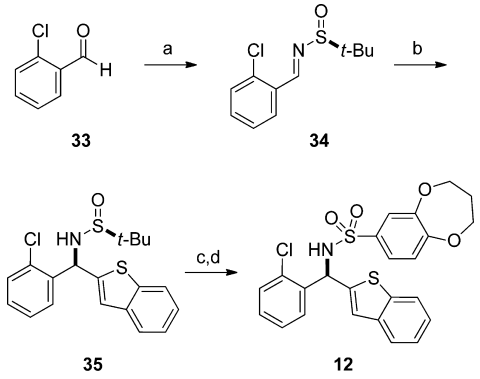

[a]Reagents and conditions: (a) (*S*)-2-methyl-2-propanesulfinamide, $Ti(OEt)_4$, CH_2Cl_2, 23 °C (88%); (b) 1-benzothiophene, *n*-butyllithium, THF, −78 °C (65%); (c) HCl, MeOH, 23 °C; (d) **10**, *i*-Pr_2NEt, DMAP, CH_2Cl_2, 23 °C (66%, two steps).

chromatography on silica gel.[39] Finally, the *tert*-butanesulfinyl group of **35** was removed (HCl/MeOH) and the resulting amine was sulfonylated using commercially available 3,4-dihydro-2*H*-1,5-benzodioxepine-7-sulfonyl chloride (**10**) to provide benzodioxepine-based diarylmethanesulfonamide **12** (66% yield, two steps).

As illustrated in Scheme 3, cyclopropane-based diarylmethanesulfonamide **25** was accessed by a similar route.

Scheme 3. Chemical Synthesis of Cyclopropane-Based GK–GKRP Disrupter 25[a]

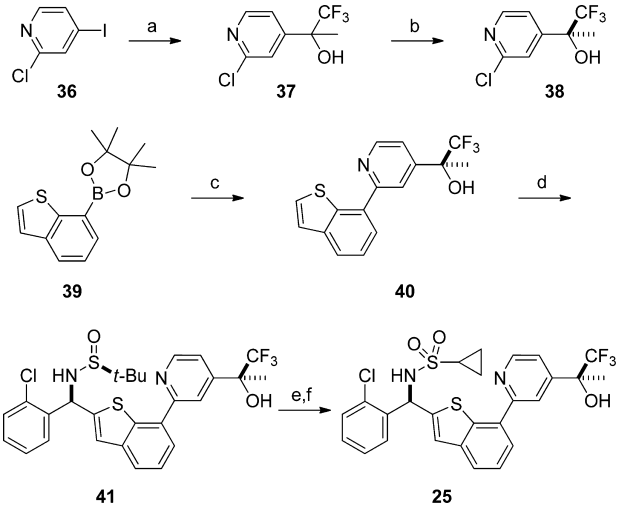

[a]Reagents and conditions: (a) *n*-butyllithium, 1,1,1-trifluoroacetone, THF, −78 °C (65%); (b) chiral SFC purification;[40] (c) **38**, $Pd(allyl)_2Cl_2$, X-Phos, $Na_2CO_3 \cdot H_2O$, 4:1 1,4-dioxane–H_2O, 80 °C (50%); (d) *n*-butyllithium (2.2 equiv), **34**, THF, −78 °C (51%); (e) HCl, Et_2O, 23 °C; (f) cyclopropanesulfonyl chloride, *i*-Pr_2NEt, DMAP, DMF, 23 °C (70%, two steps).

The synthesis of **25** showcases the standard means to the 7-arylbenzothiophene disrupters **22**–**27** in Tables 3 and 4.[38] Lithium–iodine exchange of commercially available 2-chloro-4-iodopyridine (**36**) using *n*-butyllithium followed by addition of 1,1,1-trifluoroacetone afforded racemic 2-(2-chloro-4-pyridinyl)-1,1,1-trifluoro-2-propanol (**37**) in 65% yield, which was resolved by chiral SFC to afford the enantiomerically pure *S*-configured isomer **38** and its *R*-configured antipode.[40] 2-Chloropyridine **38** was coupled with known 2-(1-benzothiophen-7-yl)-4,4,5,5-tetramethyl-1,3,2-dioxaborolane (**39**)[41] using $Pd(allyl)_2Cl_2$/X-Phos to give 7-pyridylbenzothiophene **40** in 50% yield. Selective bis-deprotonation of **40** with 2.2 equiv of *n*-butyllithium followed by addition of *tert*-butanesulfinylimine **34** gave *tert*-butanesulfinamide **41** possessing the *R* configuration at the diarylmethane stereocenter in 51% yield after removal of the minor undesired diastereomer by flash chromatography on silica gel.[39] Lastly, the *tert*-butanesulfinyl group of **41** was removed by treatment with HCl and the resulting amine was sulfonylated using commercially available cyclopropanesulfonyl chloride to provide cyclopropane-based diarylmethanesulfonamide **25** (70% yield, two steps).

The synthetic approach used to acquire phenyl analogue **25** was extended to the more complex aminopyridines **28** and **29** and aminopyrimidine **31**, as represented by the assembly of **31** in Scheme 4.[38] Commercially available 4-chloropyrimidin-2-amine (**42**) was regioselectively chlorinated with 1,3,5-trichloroisocyanuric acid, and then the amine functionality was protected as its di-*tert*-butylimidodicarbonate using Boc_2O/DMAP to provide dichloropyrimidine **43** in 53% yield for the two-step process. Regioselective palladium-catalyzed cross-coupling ($Pd(AmPhos)_2Cl_2$/KOAc) of **43** with commercially

DOI: 10.1021/acs.jmedchem.5b01367
J. Med. Chem. XXXX, XXX, XXX–XXX

Scheme 4. Chemical Synthesis of GK−GKRP Disrupter 31[a]

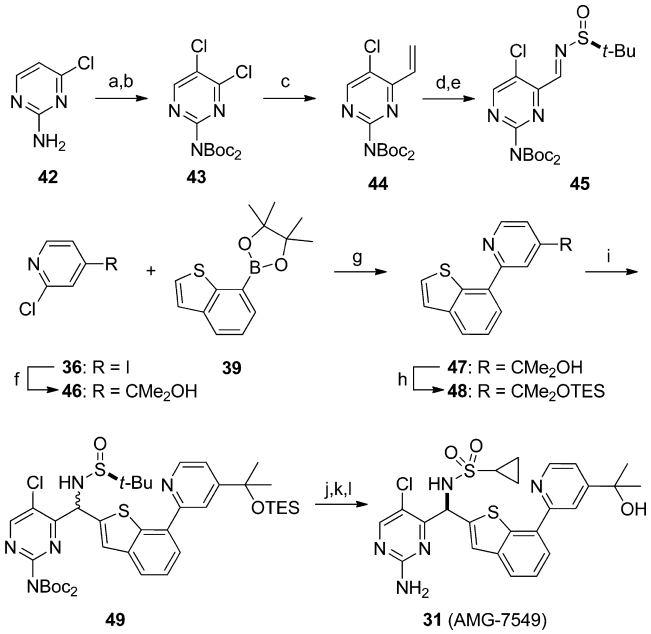

[a]Reagents and conditions: (a) 1,3,5-trichloroisocyanuric acid, AcOH, H_2O, 50 °C; (b) Boc_2O, DMAP, THF, 23 °C (53%, two steps); (c) potassium vinyltrifluoroborate, $Pd(AmPhos)_2Cl_2$, KOAc, 3:1 MeCN−H_2O, 70 °C (77%); (d) $K_2OsO_4·2H_2O$, $NaIO_4$, 4:1 THF−H_2O, 23 °C; (e) (*S*)-2-methyl-2-propanesulfinamide, $CuSO_4$, CH_2Cl_2, 23 °C (58%, two steps); (f) *n*-butyllithium, acetone, THF, −78 °C (61%); (g) $Pd(allyl)_2Cl_2$, X-Phos, Na_2CO_3, 6:1 1,4-dioxane−H_2O, 80 °C (53%); (h) Et_3SiOTf, *i*-Pr_2NEt, THF, 0 °C (88%); (i) *n*-butyllithium, LiCl, **45**, THF, −78 °C (quant, crude); (j) HCl, MeOH, 10 → 23 °C; (k) cyclopropanesulfonyl chloride, *i*-Pr_2NEt, DMAP, DMF, 13 → 23 °C (49%, three steps); (l) chiral SFC purification.[42]

available potassium vinyltrifluoroborate gave alkene **44** (77% yield). Alkene **44** was oxidatively cleaved using $K_2OsO_4/NaIO_4$ to the desired aldehyde, which was then condensed with commercially available (*S*)-2-methyl-2-propanesulfinamide using $CuSO_4$ to afford *tert*-butanesulfinylimine **45** (58% yield, two steps). Lithium−iodine exchange of commercially available 2-chloro-4-iodopyridine (**36**) using *n*-butyllithium followed by addition of acetone afforded 2-(2-chloro-4-pyridinyl)-2-propanol (**46**) in 61% yield. 2-Chloropyridine **46** was cross-coupled with **39** using $Pd(allyl)_2Cl_2$/X-Phos/Na_2CO_3 to give 2-(2-(1-benzothiophen-7-yl)-4-pyridinyl)-2-propanol (**47**) in 53% yield, the *gem*-dimethylcarbinol moiety of which was then protected as its triethylsilyl ether (Et_3SiOTf/*i*-Pr_2NEt) to afford afford 2-(1-benzothiophen-7-yl)-4-(1-methyl-1-((triethylsilyl)-oxy)ethyl)pyridine (**48**) in 88% yield. Selective deprotonation of **48** (*n*-butyllithium/LiCl) followed by addition of *tert*-butanesulfinylimine **45** gave *tert*-butanesulfinamide **49** as a ∼1:1 mixture of diastereomers at the diarylmethane stereocenter.[39] The crude material was deprotected by treatment with HCl in methanol, and the resulting diarylmethaneamine group was sulfonylated using commercially available cyclopropanesulfonyl chloride to give the final product as a ∼1:1 mixture of enantiomers (49% overall yield, three steps). The enantiomeric mixture was resolved using chiral SFC and the *R* absolute stereochemistry of **31** was assigned by comparison of its quantum mechanically computed and measured optical rotation.[42]

The aminopyridines **30** and **32** were prepared by a different route, as shown for **32** in Scheme 5.[38] Selective deprotonation

Scheme 5. Chemical Synthesis of GK−GKRP Disrupter 32[a]

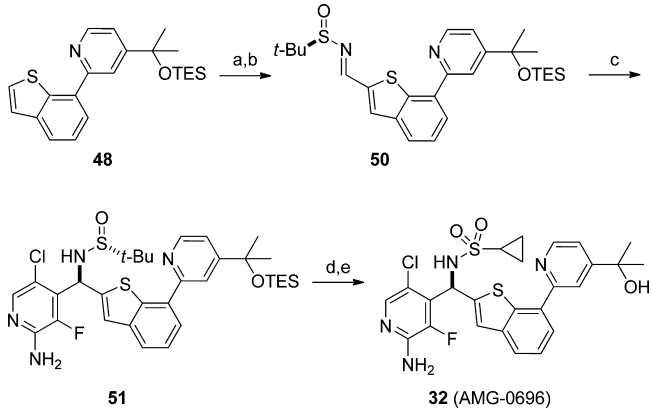

[a]Reagents and conditions: (a) *n*-butyllithium, DMF, THF, −78 °C; (b) (*R*)-2-methyl-2-propanesulfinamide, $Ti(OEt)_4$, CH_2Cl_2, 23 °C (87%, two steps); (c) 5-chloro-3-fluoro-2-pyridinamine, *n*-butyllithium (1.9 equiv), THF, −78 °C (23%); (d) HCl, MeOH, 23 °C; (e) cyclopropanesulfonyl chloride, *i*-Pr_2NEt, DMAP, DMF, 23 °C (83%, two steps).

of **48** with *n*-butyllithium followed by addition of *N*,*N*-dimethylformamide gave the desired aldehyde, which was condensed with commercially available (*R*)-2-methyl-2-propanesulfinamide using $Ti(OEt)_4$ to afford *tert*-butanesulfinylimine **50** (87% yield, two steps). Selective bis-deprotonation of commercially available 5-chloro-3-fluoro-2-pyridinamine with 1.9 equiv of *n*-butyllithium followed by addition of *tert*-butanesulfinylimine **50** gave *tert*-butanesulfinamide **51** possessing the *R* configuration at the diarylmethane stereocenter in 23% yield after removal of the minor undesired diastereomer by flash chromatography on silica gel.[39,43] Global deprotection of **51** by treatment with HCl in methanol followed by selective sulfonylation of the diarylmethaneamine group with commercially available cyclopropanesulfonyl chloride gave **32** in 83% yield for the two-step process.

CONCLUSIONS

A structurally distinct series of GKRP-selective GK−GKRP disrupters was discovered through an HTS campaign of a diverse compound library. By leveraging structure-guided drug design, benzodioxepine-based diarylmethanesulfonamide **6** was transformed into cyclopropane-based diarylmethanesulfonamide **32**. This lead optimization effort exploited an unusual N → S ($n_N \rightarrow \sigma^*_{S-X}$) interaction to conformationally constrain a key biaryl linkage. Computational studies revealed the underpinnings of the N → S ($n_N \rightarrow \sigma^*_{S-X}$) interaction, and X-ray analysis of **32** bound to GKRP confirmed its predicted binding conformation and interactions with the protein. Lead compound **32** was found to possess improved metabolic stability, as well as to induce dramatic GK translocation in Sprague−Dawley rats and robust blood glucose reduction in db/db mice. This structurally novel disrupter of GK−GKRP binding allows further exploration of the pharmacology of this potential therapeutic axis for T2DM and highlights the value of incorporating unconventional nonbonded interactions in drug design.

DOI: 10.1021/acs.jmedchem.5b01367
J. Med. Chem. XXXX, XXX, XXX−XXX

EXPERIMENTAL SECTION

Chemistry (General).[38,44] Unless otherwise indicated, all materials were obtained from commercial suppliers and used without further purification. Anhydrous solvents were obtained from Sigma–Aldrich, Acros, or EM Science and used as received. All reactions involving air- or moisture-sensitive reagents were performed under a nitrogen or argon atmosphere. All microwave-assisted reactions were performed in sealed reaction vials using a Personal Chemistry Emrys Optimizer microwave synthesizer. Silica gel chromatography was performed using either glass columns packed with silica gel (200–400 mesh, Sigma-Aldrich) or prepacked silica gel cartridges (Biotage or RediSep). All final compounds were purified to ≥95% purity unless otherwise noted, as determined by HPLC–MS obtained on an Agilent 1100 or 1200 spectrometer using the following methods: [A] Agilent SB-C18 column (50 mm × 3.0 mm, 2.5 μm) at 40 °C with a 1.5 mL/min flow rate using a gradient of 5–95% [0.1% TFA in acetonitrile] in [0.1% TFA in water] over 3.5 min; [B] Waters XBridge C18 column (50 mm × 3.0 mm, 3 μm) at 40 °C with a 1.5 mL/min flow rate using a gradient of 5–95% [0.1% formic acid in acetonitrile] in [0.1% formic acid water] over 3.5 min. NMR spectra were obtained with a Bruker 300 MHz or a DRX 400, 500, or 600 MHz spectrometer. Data are reported as follows: chemical shift in parts per million (ppm, δ units) from an internal standard, multiplicity (s = singlet, d = doublet, t = triplet, q = quartet, dd = doublet of doublets, quin = quintet, m = multiplet, and br s = broad singlet), coupling constant (Hz), and integration. Low-resolution mass spectrometry (MS) data were obtained at the same time as the purity determination with the HPLC–MS instrument using ES ionization (positive mode). High-resolution mass spectrometry (HRMS) data were obtained with a Waters Synapt G2 QTOF system operated in either positive or negative ion mode.

***N*-((*R*)-1-Benzothiophen-2-yl(2-chlorophenyl)methyl)-3,4-dihydro-2*H*-1,5-benzodioxepine-7-sulfonamide (12).** Titanium(IV) tetraethoxide (220 mL, 1100 mmol) was added to a solution of 2-chlorobenzaldehyde (**33**; 30 g, 210 mmol), (*S*)-2-methyl-2-propanesulfinamide (26 g, 210 mmol), and dichloromethane (430 mL) at room temperature. After 22 h, the reaction mixture was added to water, dichloromethane was added, the mixture was agitated vigorously, filtered through a pad of diatomaceous earth, the two layers comprising the filtrate were separated, the organic material was dried (sodium sulfate), filtered, and the filtrate was concentrated under reduced pressure. The residue was subjected to flash chromatography on silica gel (9:1 hexane–ethyl acetate) to afford *N*-((*S*,1*E*)-(2-chlorophenyl)methylidene)-2-methyl-2-propanesulfinamide (**34**; 46 g, 88% yield) as a clear yellow oil. ^{1}H NMR (400 MHz, $CDCl_3$) δ 9.05 (s, 1 H), 8.06 (d, *J* = 7.8 Hz, 1 H), 7.49–7.39 (m, 2 H), 7.38–7.31 (m, 1 H), 1.28 (s, 9 H). MS *m*/*z* 243.9 $[M + H]^+$ (244.0 calcd for $C_{11}H_{15}ClNOS^+$).

n-Butyllithium (2.6 mL of a 2.5 M solution with toluene, 6.4 mmol) was added to a solution of 1-benzothiophene (0.79 g, 5.9 mmol) and tetrahydrofuran (26 mL) at −78 °C. After 15 min, a solution of **34** (1.3 g, 5.3 mmol) and tetrahydrofuran (26 mL) was added. After 90 min, saturated aqueous ammonium chloride was added, the reaction vessel was removed from the cooling bath, and the mixture was allowed to warm to room temperature. The mixture was partitioned between ethyl acetate and more saturated aqueous ammonium chloride, the layers were separated, the organic material was washed sequentially with saturated aqueous ammonium chloride and brine, dried (sodium sulfate), filtered, and the filtrate was concentrated under reduced pressure. The residue was subjected to flash chromatography on silica gel (gradient elution; 9:1 to 4:1 to 3:1 to 2:1 hexane–ethyl acetate). The isolated material was resubjected to flash chromatography on silica gel (gradient elution; 3:1 to 2:1 hexane–ethyl acetate) to give (*S*)-*N*-((*R*)-1-benzothiophen-2-yl(2-chlorophenyl)methyl)-2-methyl-2-propanesulfinamide (**35**; 1.3 g, 65% yield) as a colorless solid. ^{1}H NMR (400 MHz, DMSO-d_6) δ 7.94–7.86 (m, 1 H), 7.83 (dd, *J* = 1.5, 7.7 Hz, 1 H), 7.79–7.70 (m, 1 H), 7.53–7.42 (m, 2 H), 7.42–7.35 (m, 1 H), 7.35–7.26 (m, 2 H), 7.02 (s, 1 H), 6.61 (d, *J* = 7.1 Hz, 1 H), 6.15 (d, *J* = 7.1 Hz, 1 H), 1.18 (s, 9 H). MS *m*/*z* 377.9 $[M + H]^+$ (378.1 calcd for $C_{19}H_{21}ClNOS_2^+$).

Hydrogen chloride (1.7 mL of a 4.0 M solution with 1,4-dioxane, 6.9 mmol) was added to a solution of **35** (1.3 g, 3.4 mmol) and methanol (3.4 mL) at room temperature. After 80 min, the reaction mixture was concentrated under reduced pressure, diethyl ether was added to the residue, the resulting slurry was subjected to sonication for 5 min, filtered, and the filter cake was collected to afford (*R*)-1-(1-benzothiophen-2-yl)-1-(2-chlorophenyl)methanamine hydrochloride (0.90 g, 85% yield) as an off-white solid. The material was used in the next step of the synthesis without purification.

(*R*)-1-(1-Benzothiophen-2-yl)-1-(2-chlorophenyl)methanamine hydrochloride (0.10 g, 0.32 mmol) was dissolved with dichloromethane (3.2 mL) and diisopropylethylamine (0.17 mL, 0.97 mmol), and then 3,4-dihydro-2*H*-1,5-benzodioxepine-7-sulfonyl chloride (**10**; 0.080 g, 0.32 mmol) was added. After 2 h, 4-dimethylaminopyridine (0.0039 g, 0.032 mmol) was added. After 3 h, more diisopropylethylamine (0.17 mL, 0.97 mmol) was added. After 30 min, more **10** (0.080 g, 0.32 mmol) was added. After 23 h, the reaction mixture was partitioned between ethyl acetate and saturated aqueous sodium bicarbonate, the layers were separated, the organic material was washed sequentially with saturated aqueous sodium bicarbonate and brine, dried (sodium sulfate), filtered, and the filtrate was concentrated under reduced pressure. The residue was subjected to flash chromatography on silica gel (4:1 hexane–ethyl acetate) to give *N*-((*R*)-1-benzothiophen-2-yl(2-chlorophenyl)methyl)-3,4-dihydro-2*H*-1,5-benzodioxepine-7-sulfonamide (**12**; 0.12 g, 77% yield; 66% yield, two steps) as a colorless solid. $[\alpha]^{30}_D$ +14.2° (*c* 1.16, $CHCl_3$). ^{1}H NMR (400 MHz, DMSO-d_6) δ 9.16 (br s, 1 H), 7.93–7.84 (m, 1 H), 7.75–7.66 (m, 1 H), 7.56–7.49 (m, 1 H), 7.42–7.35 (m, 1 H), 7.35–7.22 (m, 4 H), 7.20 (dd, *J* = 2.2, 8.5 Hz, 1 H), 7.09 (d, *J* = 2.3 Hz, 1 H), 6.88 (d, *J* = 8.4 Hz, 1 H), 6.82 (s, 1 H), 6.16 (br s, 1 H), 4.17–3.96 (m, 4 H), 2.08 (quin, *J* = 5.6 Hz, 2 H). ^{13}C NMR (150 MHz, DMSO-d_6) δ 153.9, 149.9, 144.4, 139.0, 138.7, 136.8, 134.6, 131.5, 129.4, 129.0, 128.6, 127.4, 124.5, 124.4, 123.7, 122.3, 122.2, 121.8, 121.5, 119.9, 70.2, 70.1, 53.6, 30.4. HRMS *m*/*z* 484.0443 $[M - H]^-$ (484.0444 calcd for $C_{24}H_{19}ClNO_4S_2^-$).

***N*-((*R*)-(2-Chlorophenyl)(7-(4-((1*S*)-2,2,2-trifluoro-1-hydroxy-1-methylethyl)-2-pyridinyl)-1-benzothiophen-2-yl)methyl)-cyclopropanesulfonamide (25).** *n*-Butyllithium (33 mL of a 2.5 M solution with toluene, 83 mmol) was added to a solution of 2-chloro-4-iodopyridine (**36**; 20 g, 82 mmol) and tetrahydrofuran (200 mL) at −78 °C. After 15 min, 1,1,1-trifluoroacetone (28 g, 250 mmol) was added. After 1 h, saturated aqueous ammonium chloride was added, the reaction vessel was removed from the cooling bath, the reaction mixture was allowed to warm to room temperature, partitioned between more saturated aqueous ammonium chloride and ethyl acetate, the layers were separated, the aqueous material was washed with ethyl acetate (2×), the combined organic extract was washed sequentially with water and brine, dried (sodium sulfate), filtered, and the filtrate was concentrated under reduced pressure. The residue was subjected to flash chromatography on silica gel (19:1 hexane–ethyl acetate) to give racemic 2-(2-chloro-4-pyridinyl)-1,1,1-trifluoro-2-propanol (**37**; 12 g, 65% yield) as a pale yellow solid. ^{1}H NMR (400 MHz, DMSO-d_6) δ 8.63 (d, *J* = 5.1 Hz, 1 H), 7.91 (s, 1 H), 7.81 (d, *J* = 5.1 Hz, 1 H), 2.63 (s, 3 H); one exchangeable proton was not observed. MS *m*/*z* 225.9 $[M + H]^+$ (226.0 calcd for $C_8H_8ClF_3NO^+$).

Racemate **37** was resolved using preparative chiral SFC (two 250 mm × 30 mm, 5 μm Chiralcel OJ-H columns in series), eluting with 90% liquid CO_2 in 10% mixture of hexanes/isopropanol (75:25 v/v) containing 20 mM ammonia in methanol at a flow rate of 120 mL/min) to give two products in >98% enantiomeric excess. First eluting peak: (2*R*)-2-(2-chloro-4-pyridinyl)-1,1,1-trifluoro-2-propanol. Second eluting peak: (2*S*)-2-(2-chloro-4-pyridinyl)-1,1,1-trifluoro-2-propanol (**38**).[40] ^{1}H NMR (400 MHz, methanol-d_4) δ 8.40 (d, *J* = 5.3 Hz, 1 H), 7.69 (s, 1 H), 7.59 (d, *J* = 5.3 Hz, 1 H), 1.73 (s, 3 H); one exchangeable proton was not observed. MS *m*/*z* 225.9 $[M + H]^+$ (226.0 calcd for $C_8H_8ClF_3NO^+$).

A mixture of **38** (1.1 g, 4.7 mmol), 2-(1-benzothiophen-7-yl)-4,4,5,5-tetramethyl-1,3,2-dioxaborolane (**39**; 2.1 g, 8.1 mmol),[41]

DOI: 10.1021/acs.jmedchem.5b01367
J. Med. Chem. XXXX, XXX, XXX–XXX

dicyclohexyl(2′,4′,6′-tris(1-methylethyl)-2-biphenylyl)phosphane (0.23 g, 0.47 mmol), chloro(2-propen-1-yl)palladium dimer (0.087 g, 0.24 mmol), sodium carbonate monohydrate (1.8 g, 14 mmol), 1,4-dioxane (8.0 mL), and water (2.0 mL) was stirred at 80 °C for 7 h and then at room temperature for 14 h. The reaction mixture was concentrated under reduced pressure, and then the residue was subjected to flash chromatography on silica gel (gradient elution; 9:1 to 7:3 hexane−ethyl acetate). The isolated material was resubjected to flash chromatography on silica gel (gradient elution; 9:1 to 7:3 hexane−ethyl acetate) to give (2*S*)-2-(2-(1-benzothiophen-7-yl)-4-pyridinyl)-1,1,1-trifluoro-2-propanol (**40**; 0.77 g, 50% yield) as a colorless oil. ^{1}H NMR (300 MHz, $CDCl_3$) δ 8.85 (dd, J = 0.9, 5.3 Hz, 1 H), 8.20−8.16 (m, 1 H), 7.92 (d, J = 7.6 Hz, 2 H), 7.60−7.40 (m, 4 H), 2.72 (s, 1 H), 1.84 (dd, J = 0.3, 0.9 Hz, 3 H). MS m/z 324.0 $[M + H]^+$ (324.1 calcd for $C_{16}H_{13}F_3NOS^+$).

n-Butyllithium (3.2 mL of a 1.6 M solution with hexanes, 5.1 mmol) was added to a solution of **40** (0.76 g, 2.3 mmol) and tetrahydrofuran (2.0 mL) at −78 °C. After 30 min, a solution of **34** (0.74 g, 3.0 mmol) and tetrahydrofuran (1.0 mL) at −78 °C was added dropwise via a cannula. After 3 h, saturated aqueous ammonium chloride was added, the cooling bath was removed, the mixture was allowed to warm to room temperature, partitioned between more aqueous ammonium chloride and ethyl acetate, the layers were separated, the aqueous material was washed with ethyl acetate (2×), the combined organic material was dried (magnesium sulfate), filtered, and the filtrate was concentrated under reduced pressure. The residue was subjected to flash chromatography on silica gel (gradient elution; 9:1 to 2:3 hexane−ethyl acetate). The isolated material was resubjected to flash chromatography on silica gel (gradient elution; 7:3 to 2:3 hexane−ethyl acetate) to provide (*S*)-*N*-((*R*)-(2-chlorophenyl)(7-(4-((1*S*)-2,2,2-trifluoro-1-hydroxy-1-methylethyl)-2-pyridinyl)-1-benzothiophen-2-yl)methyl)-2-methyl-2-propanesulfinamide (**41**; 0.67 g, 51% yield) as a light yellow solid. ^{1}H NMR (400 MHz, $CDCl_3$) δ 8.89−8.66 (m, 1 H), 8.14 (s, 1 H), 7.86 (d, J = 7.4 Hz, 1 H), 7.75 (d, J = 7.8 Hz, 1 H), 7.65 (d, J = 7.6 Hz, 1 H), 7.49−7.41 (m, 2 H), 7.38 (d, J = 7.8 Hz, 1 H), 7.34−7.28 (m, 1 H), 7.27−7.19 (m, 2 H), 6.36 (d, J = 5.1 Hz, 1 H), 4.14 (d, J = 5.3 Hz, 1 H), 3.15 (br s, 1 H), 1.81 (s, 3 H), 1.31 (s, 9 H). MS m/z 566.7 $[M + H]^+$ (567.1 calcd for $C_{27}H_{27}ClF_3N_2O_2S_2^+$).

Hydrogen chloride (2.9 mL of a 2.0 M solution with diethyl ether, 5.8 mmol) was added to a solution of **41** (0.66 g, 1.2 mmol) and diethyl ether (8.0 mL). After 6 h, the reaction mixture was filtered, and then the filter cake was washed with diethyl ether and dried under reduced pressure. The solid was dissolved with 2.0 M ammonia in methanol and dichloromethane, silica gel was added, and the volatiles were removed under reduced pressure. The residue was subjected to flash chromatography on silica gel (gradient elution; 7:3 to 3:7 hexane−ethyl acetate) to yield (2*S*)-2-(2-(2-((*R*)-amino(2-chlorophenyl)methyl)-1-benzothiophen-7-yl)-4-pyridinyl)-1,1,1-trifluoro-2-propanol (0.51 g, 92% yield) as a colorless solid. ^{1}H NMR (400 MHz, $CDCl_3$) δ 8.82 (d, J = 5.3 Hz, 1 H), 8.13 (s, 1 H), 7.88−7.80 (m, 1 H), 7.77−7.70 (m, 1 H), 7.62 (dd, J = 1.7, 7.7 Hz, 1 H), 7.48−7.41 (m, 2 H), 7.38 (dd, J = 1.4, 7.8 Hz, 1 H), 7.31−7.26 (m, 1 H), 7.24−7.19 (m, 1 H), 7.17 (d, J = 0.8 Hz, 1 H), 5.96 (s, 1 H), 1.83 (s, 3 H); two exchangeable protons were not observed. MS m/z 462.8 $[M + H]^+$ (463.1 calcd for $C_{23}H_{19}ClF_3N_2OS^+$).

4-Dimethylaminopyridine (0.0013 g, 0.011 mmol) was added to a mixture of (2*S*)-2-(2-(2-((*R*)-amino(2-chlorophenyl)methyl)-1-benzothiophen-7-yl)-4-pyridinyl)-1,1,1-trifluoro-2-propanol (0.049 g, 0.11 mmol), cyclopropanesulfonyl chloride (13 μL, 0.13 mmol), diisopropylethylamine (55 μL, 0.32 mmol), and *N*,*N*-dimethylformamide (0.70 mL). After 24 h, the mixture was diluted with methanol (1.0 mL), the solution was filtered, and the filtrate was subjected to reverse-phase HPLC (Phenomenex Gemini-NX C18 110 Å, 100 mm × 50 mm, 10 μm, 10−95% H_2O/MeCN with 0.1% TFA). The product-containing fractions were combined, neutralized with solid sodium bicarbonate, and extracted with dichloromethane (2×). The combined organic material was dried (magnesium sulfate), filtered, and the filtrate was concentrated under reduced pressure to give *N*-((*R*)-(2-chlorophenyl)(7-(4-((1*S*)-2,2,2-trifluoro-1-hydroxy-1-methylethyl)-2-pyridinyl)-1-benzothiophen-2-yl)methyl)cyclopropanesulfonamide (**25**; 0.047 g, 76% yield; 70% yield, two steps) as a colorless solid. $[\alpha]^{30}_D$ −40.4° (*c* 0.70, $CHCl_3$). ^{1}H NMR (400 MHz, $CDCl_3$) δ 8.83 (d, J = 5.3 Hz, 1 H), 8.15 (s, 1 H), 7.89 (d, J = 7.4 Hz, 1 H), 7.75 (d, J = 7.8 Hz, 1 H), 7.65 (dd, J = 1.4, 7.6 Hz, 1 H), 7.51−7.41 (m, 3 H), 7.41−7.30 (m, 2 H), 7.08 (s, 1 H), 6.42 (d, J = 8.0 Hz, 1 H), 5.44 (d, J = 8.0 Hz, 1 H), 2.31−2.24 (m, 1 H), 1.85 (s, 3 H), 1.22−1.07 (m, 2 H), 0.92−0.83 (m, 1 H), 0.82−0.72 (m, 1 H); one exchangeable proton was not observed. ^{13}C NMR (150 MHz, $CDCl_3$) δ 156.3, 148.6, 148.2, 146.8, 141.0, 138.0, 137.6, 133.0, 132.7, 130.3, 129.7, 129.2, 127.4, 125.1 (q, J = 285.6 Hz), 125.0, 124.8, 123.1, 122.4, 119.5, 118.1, 74.5 (q, J = 29.5 Hz), 55.7, 31.4, 23.8, 6.0, 5.9. HRMS m/z 567.0784 $[M + H]^+$ (567.0785 calcd for $C_{26}H_{23}ClF_3N_2O_3S_2^+$).

***N*-((*R*)-(2-Amino-5-chloro-4-pyrimidinyl)(7-(4-(1-hydroxy-1-methylethyl)-2-pyridinyl)-1-benzothiophen-2-yl)methyl)-cyclopropanesulfonamide (31).** A solution of 1,3,5-trichloroisocyanuric acid (37 g, 160 mmol), 4-chloropyrimidin-2-amine (**42**; 42 g, 320 mmol), water (380 mL), and acetic acid (42 mL) was heated at 50 °C. After 15 h, the heating bath was removed and the reaction mixture was allowed to cool to room temperature, added to crushed ice, and then the mixture was basified with 10 M aqueous sodium hydroxide. After 4 h, the mixture was filtered, and the filter cake was washed with water. The solid was suspended in 0.50 M aqueous sodium hydroxide, and the resulting mixture was stirred for 2 h. The mixture was filtered, the filter cake was washed with water and then dried under reduced pressure at elevated temperature (60 °C) to give 4,5-dichloro-2-pyrimidinamine (38 g, 73% yield) as a yellow solid. The material was used in the next step of the synthesis without purification.

A solution of 4,5-dichloro-2-pyrimidinamine (38 g, 230 mmol), tetrahydrofuran (750 mL), and 4-dimethylaminopyridine (1.4 g, 12 mmol) was treated dropwise with a solution of di-*tert*-butyl dicarbonate (120 g, 540 mmol) and tetrahydrofuran (250 mL). After 60 h, the reaction mixture was partitioned between ethyl acetate and saturated aqueous ammonium chloride, the layers were separated, the organic material was washed sequentially with water and brine, dried (magnesium sulfate), filtered, and the filtrate was concentrated under reduced pressure. The isolated solid was recrystallized (5:1 hexanes−diethyl ether) to give di-*tert*-butyl (4,5-dichloro-2-pyrimidinyl)imidodicarbonate (**43**; 62 g, 53% yield, two steps) as a yellow solid. ^{1}H NMR (400 MHz, $CDCl_3$) δ 8.67 (s, 1 H), 1.48 (s, 18 H). MS m/z 385.8 $[M + Na]^+$ (386.1 calcd for $C_{14}H_{19}Cl_2N_3NaO_4^+$).

A solution of **43** (32 g, 87 mmol), 1,1-bis[(di-*tert*-butyl-*p*-methylaminophenyl]palladium(II) chloride (2.5 g, 3.5 mmol), potassium vinyltrifluoroborate (15 g, 110 mmol), and potassium acetate (26 g, 260 mmol), acetonitrile (300 mL), and water (100 mL) was purged with nitrogen for 5 min and then heated at 70 °C. After 3 h, the heating bath was removed and the reaction mixture was allowed to cool to room temperature, partitioned between ethyl acetate and water, the layers were separated, the organic material was washed sequentially with 1.0 N aqueous HCl and brine, dried (magnesium sulfate), filtered, and the filtrate was concentrated under reduced pressure. The isolated material was subjected to flash chromatography on silica gel (gradient elution; 19:1 to 3:1 hexane−ethyl acetate) to afford di-*tert*-butyl (5-chloro-4-ethenyl-2-pyrimidinyl)-imidodicarbonate (**44**; 24 g, 77% yield) as a yellow solid. ^{1}H NMR (400 MHz, $CDCl_3$) δ 8.65 (s, 1 H), 7.15 (dd, J = 10.6, 16.8 Hz, 1 H), 6.76 (dd, J = 1.8, 16.8 Hz, 1 H), 5.84 (dd, J = 1.8, 10.6 Hz, 1 H), 1.49 (s, 18 H). MS m/z 378.1 $[M + Na]^+$ (378.1 calcd for $C_{16}H_{22}ClN_3NaO_4^+$).

Potassium osmate dihydrate (0.099 g, 0.27 mmol) was added to a solution of **44** (24 g, 67 mmol), sodium periodate (40 g, 190 mmol), tetrahydrofuran (400 mL), and water (100 mL) at room temperature. After 18 h, more potassium osmate dihydrate (0.050 g, 0.14 mmol) was added. After 4 h, Na_2SO_3 (30 g) and water (400 mL) were added. After 45 min, ethyl acetate was added, the layers were separated, the aqueous material was washed with ethyl acetate, the combined organic material was washed sequentially with water and brine, dried (magnesium sulfate), filtered, and the filtrate was concentrated under reduced pressure to afford di-*tert*-butyl (5-chloro-4-formyl-2-

DOI: 10.1021/acs.jmedchem.5b01367
J. Med. Chem. XXXX, XXX, XXX−XXX

pyrimidinyl)imidodicarbonate (24 g, quant yield) as a thick oil. The material was used in the next step of the synthesis without purification.

A mixture of di-*tert*-butyl (5-chloro-4-formyl-2-pyrimidinyl)-imidodicarbonate (24 g, 67 mmol), (*S*)-2-methyl-2-propanesulfinamide (9.8 g, 80 mmol), copper(II) sulfate (32 g, 200 mmol), and dichloromethane (200 mL) was stirred at room temperature. After 15 h, the reaction mixture was filtered through a plug of diatomaceous earth, the filter cake was washed with dichloromethane, and the filtrate was concentrated under reduced pressure. The residue was subjected to flash chromatography on silica gel (gradient elution; 19:1 to 7:3 hexane−ethyl acetate) to afford di-*tert*-butyl (4-((*E*)-(((*S*)-*tert*-butylsulfinyl)imino)methyl)-5-chloro-2-pyrimidinyl)imidodicarbonate (**45**; 18 g, 58% yield, two steps) as a yellow solid. ^{1}H NMR (400 MHz, $CDCl_3$) δ 8.85 (s, 1 H), 8.83 (s, 1 H), 1.47 (s, 18 H), 1.31 (s, 9 H). MS m/z 483.0 $[M + Na]^+$ (483.2 calcd for $C_{19}H_{29}ClN_4NaO_5S^+$).

n-Butyllithium (8.4 mL of a 2.5 M solution with toluene, 21 mmol) was added to a solution of 2-chloro-4-iodopyridine (**36**; 5.0 g, 21 mmol) and tetrahydrofuran (50 mL) at −78 °C. After 15 min, acetone (4.6 mL, 63 mmol) was added. After 1 h, saturated aqueous ammonium chloride was added, the cooling bath was removed, the mixture was allowed to warm to room temperature, partitioned between more saturated aqueous ammonium chloride and ethyl acetate, the layers were separated, the aqueous material was washed with ethyl acetate (2×), the combined organic material was washed sequentially with water and brine, dried (sodium sulfate), filtered, and the filtrate was concentrated under reduced pressure. The residue was subjected to flash chromatography on silica gel (6:1 hexane−ethyl acetate) to give 2-(2-chloro-4-pyridinyl)-2-propanol (**46**; 2.2 g, 61% yield) as a colorless solid. ^{1}H NMR (400 MHz, DMSO-d_6) δ 8.33 (d, J = 5.2 Hz, 1 H), 7.53 (s, 1 H), 7.47 (dd, J = 1.2, 4.8 Hz, 1 H), 5.42 (s, 1 H), 1.41 (s, 6 H). MS m/z 172.1 $[M + H]^+$ (172.0 calcd for $C_8H_{11}ClNO^+$).

A stirring mixture of **46** (24 g, 0.14 mol), 2-(1-benzothiophen-7-yl)-4,4,5,5-tetramethyl-1,3,2-dioxaborolane (**39**; 40 g, 0.15 mol), 1,4-dioxane (190 mL), water (30 mL), allylpalladium(II) chloride dimer (2.5 g, 7.0 mmol), 2-(dicyclohexylphosphino)-2′,4′,6′,-triisopropyl-1,1′-biphenyl (6.7 g, 14 mmol), and sodium carbonate (45 g, 0.042 mol) was heated at 80 °C. After 12 h, the heating bath was removed, the reaction mixture was allowed to cool to room temperature, filtered through a pad of diatomaceous earth, and the filtrate was concentrated under reduced pressure. The residue was partitioned between water and ethyl acetate, the layers were separated, the aqueous material was washed with ethyl acetate (2×), the combined organic extract was washed sequentially with water and brine, dried (sodium sulfate), filtered, and the filtrate was concentrated under reduced pressure. The residue was subjected to flash chromatography on silica gel (9:1 hexane−ethyl acetate) to give 2-(2-(1-benzothiophen-7-yl)-4-pyridinyl)-2-propanol (**47**; 20 g, 53% yield) as a pale yellow solid. ^{1}H NMR (400 MHz, DMSO-d_6) δ 8.71 (d, J = 5.2 Hz, 1 H), 8.23 (s, 1 H), 8.12 (d, J = 7.6 Hz, 1 H), 7.99 (d, J = 8.0 Hz, 1 H), 7.82 (d, J = 5.6 Hz, 1 H), 7.60−7.47 (m, 3 H), 5.39 (s, 1 H), 1.51 (s, 6 H). MS m/z 270.0 $[M + H]^+$ (270.1 calcd for $C_{16}H_{16}NOS^+$).

A solution of triethylsilyl trifluoromethanesulfonate (32 mL, 140 mmol) and tetrahydrofuran (50 mL) was added to a solution of **47** (30 g, 110 mmol), diisopropylethylamine (29 mL, 170 mmol), and tetrahydrofuran (100 mL) at 0 °C. After 3 h, the reaction mixture was partitioned between diethyl ether and 1.0 M aqueous KH_2PO_4, the layers were separated, the organic material was washed with brine, dried (magnesium sulfate), filtered, and the filtrate was concentrated under reduced pressure. The residue was subjected to flash chromatography on silica gel (gradient elution; hexane to 9:1 hexane−ethyl acetate) to afford 2-(1-benzothiophen-7-yl)-4-(1-methyl-1-((triethylsilyl)oxy)ethyl)pyridine (**48**; 37 g, 88% yield) as a colorless oil. ^{1}H NMR (400 MHz, $CDCl_3$) δ 8.77−8.72 (m, 1 H), 8.08 (d, J = 0.8 Hz, 1 H), 7.89 (d, J = 7.6 Hz, 2 H), 7.56 (d, J = 5.7 Hz, 1 H), 7.50 (t, J = 7.6 Hz, 1 H), 7.41 (d, J = 5.7 Hz, 1 H), 7.34 (dd, J = 1.7, 5.2 Hz, 1 H), 1.63 (s, 6 H), 1.00 (t, J = 7.9 Hz, 9 H), 0.71−0.64 (m, 6 H). MS m/z 384.1 $[M + H]^+$ (384.2 calcd for $C_{22}H_{30}NOSSi^+$).

n-Butyllithium (22 mL of a 2.5 M solution with hexanes, 55 mmol) was added to a solution of **48** (19 g, 50 mmol) and lithium chloride (200 mL of a 0.50 M solution with tetrahydrofuran, 99 mmol) at −78 °C. After 30 min, the mixture was added via cannula over 10 min to a solution of **45** (23 g, 50 mmol) and tetrahydrofuran (200 mL) at −78 °C. After 20 min, saturated aqueous ammonium chloride was added slowly, the mixture was partitioned between ethyl acetate and 5.0% aqueous sodium bicarbonate, the layers were separated, the aqueous material was washed with ethyl acetate, the combined organic material was washed with brine (2×), dried (magnesium sulfate), filtered, and the filtrate was concentrated under reduced pressure to afford a ∼1:1 diastereomeric mixture of di-*tert*-butyl (4-((((*S*)-*tert*-butylsulfinyl)-amino)(7-(4-(1-methyl-1-((triethylsilyl)oxy)ethyl)-2-pyridinyl)-1-benzothiophen-2-yl)methyl)-5-chloro-2-pyrimidinyl)imidodicarbonate (**49**; 42 g, quant yield) as an amber oil. The material was used in the next step of the synthesis without purification.

Hydrogen chloride (200 mL of a 4.0 M solution with 1,4-dioxane, 790 mmol) was added to a stirring suspension of **49** (42 g, 50 mmol) and methanol (200 mL) at 10 °C, and then the cooling bath was removed and the reaction mixture was allowed to warm to room temperature. After 72 h, diethyl ether was added over a 90 min period. The mixture was filtered and the filter cake was washed with diethyl ether to afford ∼1:1 enantiomeric mixture of 2-(2-(2-(amino(2-amino-5-chloro-4-pyrimidinyl)methyl)-1-benzothiophen-7-yl)-4-pyridinyl)-2-propanol trihydrochloride (17 g, 65% yield) as a pale yellow solid. The material was used in the next step of the synthesis without purification.

Cyclopropanesulfonyl chloride (4.9 mL, 49 mmol) was added to a stirring solution of a ∼1:1 enantiomeric mixture of 2-(2-(2-(amino(2-amino-5-chloro-4-pyrimidinyl)methyl)-1-benzothiophen-7-yl)-4-pyridinyl)-2-propanol trihydrochloride (17 g, 32 mmol), 4-dimethylaminopyridine (0.40 g, 3.2 mmol), diisopropylethylamine (23 mL, 130 mmol), and *N*,*N*-dimethylformamide (100 mL) at 13 °C, and then the cooling bath was removed and the reaction mixture was allowed to warm to room temperature. After 18 h, the reaction mixture was partitioned between ethyl acetate and 5.0% aqueous sodium bicarbonate, the layers were separated, the organic material was washed sequentially with water (2×) and brine, dried (magnesium sulfate), filtered, and the filtrate was concentrated under reduced pressure. The residue was suspended in 9:1 dichloromethane−isopropanol, the suspension was filtered, and then the filter cake was washed with diethyl ether and collected to afford the desired product (2.1 g) as white solid. Silica gel was added to the filtrate, the volatiles were removed under reduced pressure, and the residue was subjected to flash chromatography on silica gel (gradient elution; 49:1 to 19:1 dichloromethane−2.0 M NH_3 in methanol). The isolated materials were combined to afford a ∼1:1 enantiomeric mixture of *N*-((2-amino-5-chloro-4-pyrimidinyl)(7-(4-(1-hydroxy-1-methylethyl)-2-pyridinyl)-1-benzothiophen-2-yl)methyl)cyclopropanesulfonamide (13 g, 49% yield, three steps) as a tan solid. The combined material was subjected to preparative chiral SFC (Chiralpak AD-H column; 25 cm × 30 mm, 5 μm) eluting with 60% liquid CO_2 in 40% isopropanol (with 20 mM NH_3) at a flow rate of 120 mL/min) to afford two products in >99% enantiomeric excess. First eluting peak: *N*-((*S*)-(2-amino-5-chloro-4-pyrimidinyl)(7-(4-(1-hydroxy-1-methylethyl)-2-pyridinyl)-1-benzothiophen-2-yl)methyl)cyclopropanesulfonamide. Second eluting peak: *N*-((*R*)-(2-amino-5-chloro-4-pyrimidinyl)(7-(4-(1-hydroxy-1-methylethyl)-2-pyridinyl)-1-benzothiophen-2-yl)methyl)cyclopropanesulfonamide (**31**)[42] as a tan solid. $[\alpha]^{20}_D$ +48.3° (*c* 0.39, MeOH). ^{1}H NMR (400 MHz, DMSO-d_6) δ 8.71 (d, J = 5.1 Hz, 1 H) 8.34 (s, 1 H) 8.21 (s, 1 H) 8.10 (d, J = 8.6 Hz, 2 H) 7.94−7.85 (m, 1 H) 7.58−7.44 (m, 2 H) 7.33 (d, J = 1.0 Hz, 1 H) 6.98 (br s, 2 H) 6.09 (dd, J = 0.9, 8.9 Hz, 1 H) 5.35 (br s, 1 H) 2.45−2.33 (m, 1 H) 1.50 (s, 6 H) 0.97−0.79 (m, 3 H) 0.78−0.68 (m, 1 H). ^{13}C NMR (100 MHz, DMSO-d_6) δ 163.0, 162.0, 160.4, 158.0, 154.6, 148.0, 145.0, 140.5, 136.4, 132.6, 124.8, 124.8, 122.7, 122.3, 119.0, 116.6, 114.8, 70.6, 54.0, 31.2, 30.8, 5.3, 4.9. HRMS m/z 530.1086 $[M + H]^+$ (530.1087 calcd for $C_{24}H_{25}ClN_5O_3S_2^+$).

***N*-((*R*)-(2-Amino-5-chloro-3-fluoro-4-pyridinyl)(7-(4-(1-hydroxy-1-methylethyl)-2-pyridinyl)-1-benzothiophen-2-yl)-methyl)cyclopropanesulfonamide (32).** *n*-Butyllithium (23 mL of a 2.5 M solution with toluene, 57 mmol) was added to a solution of 2-(1-benzothiophen-7-yl)-4-(1-methyl-1-((triethylsilyl)oxy)ethyl)-

DOI: 10.1021/acs.jmedchem.5b01367
J. Med. Chem. XXXX, XXX, XXX−XXX

pyridine (**48**; 22 g, 57 mmol) and tetrahydrofuran (120 mL) at −78 °C. After 30 min, *N*,*N*-dimethylformamide (22 mL, 290 mmol) was added. After 40 min, saturated aqueous sodium bicarbonate and ethyl acetate were added, the layers were separated, the organic material was washed sequentially with saturated aqueous sodium bicarbonate and brine, dried (sodium sulfate), filtered, and the filtrate was concentrated under reduced pressure to give 7-(4-(1-methyl-1-((triethylsilyl)oxy)-ethyl)-2-pyridinyl)-1-benzothiophene-2-carbaldehyde (24 g, quant yield) as an off-white solid. The material was used in the next step of the synthesis without purification.

Titanium tetraethoxide (61 mL, 290 mmol) was added to a stirring solution of 7-(4-(1-methyl-1-((triethylsilyl)oxy)ethyl)-2-pyridinyl)-1-benzothiophene-2-carbaldehyde (24 g, 58 mmol), (*R*)-2-methyl-2-propanesulfinamide (7.1 g, 58 mmol), and dichloromethane (120 mL) at room temperature. After 13 h, the reaction mixture was partitioned between water and dichloromethane, the layers were separated, the aqueous material was washed with dichloromethane, the combined organic material was dried (sodium sulfate), filtered, and the filtrate was concentrated. The residue was subjected to flash chromatography on silica gel (5:1 hexane−ethyl acetate) to give (*R*)-2-methyl-*N*-((1*E*)-(7-(4-(1-methyl-1-((triethylsilyl)oxy)ethyl)-2-pyridinyl)-1-benzothiophen-2-yl)methylidene)-2-propanesulfinamide (**50**; 26 g, 87% yield, two steps) as a yellow solid. ^{1}H NMR (400 MHz, $CDCl_3$) δ 8.85 (s, 1 H), 8.81−8.73 (m, 1 H), 8.08 (s, 1 H), 8.02−7.96 (m, 1 H), 7.96−7.90 (m, 1 H), 7.84 (s, 1 H), 7.54 (t, J = 7.7 Hz, 1 H), 7.35 (dd, J = 1.7, 5.2 Hz, 1 H), 1.63 (s, 6 H), 1.30 (s, 9 H), 1.00 (t, J = 7.9 Hz, 9 H), 0.67 (q, J = 7.9 Hz, 6 H). MS m/z 515.1 $[M + H]^+$ (515.2 calcd for $C_{27}H_{39}N_2O_2S_2Si^+$).

n-Butyllithium (32 mL of a 2.5 M solution with toluene, 80 mmol) was added slowly to a solution of 5-chloro-3-fluoro-2-pyridinamine (6.3 g, 43 mmol) and tetrahydrofuran (80 mL) at −78 °C. After 2 h, a solution of **50** (10 g, 19 mmol) and tetrahydrofuran (17 mL) was added slowly. After 80 min, saturated aqueous sodium bicarbonate was added, the cooling bath was removed, the mixture was allowed to warm to room temperature, partitioned between ethyl acetate and more saturated aqueous sodium bicarbonate, the layers were separated, the organic material was washed with brine, dried (sodium sulfate), filtered, and the filtrate was concentrated under reduced pressure. The residue was subjected to flash chromatography on silica gel (gradient elution; 5:1 to 3:1 hexane−acetone). The isolated material was resubjected to flash chromatography on silica gel (1:1 hexane−ethyl acetate) to give (*R*)-*N*-((*R*)-(2-amino-5-chloro-3-fluoro-4-pyridinyl)-(7-(4-(1-methyl-1-((triethylsilyl)oxy)ethyl)-2-pyridinyl)-1-benzothiophen-2-yl)methyl)-2-methyl-2-propanesulfinamide (**51**; 2.9 g, 23% yield) as a pale yellow solid. ^{1}H NMR (400 MHz, DMSO-d_6) δ 8.70 (d, J = 5.3 Hz, 1 H), 8.17 (s, 1 H), 8.04 (d, J = 6.9 Hz, 1 H), 7.93 (d, J = 7.2 Hz, 1 H), 7.89 (s, 1 H), 7.54 (t, J = 7.6 Hz, 1 H), 7.50−7.43 (m, 1 H), 6.51 (s, 2 H), 6.38 (d, J = 7.4 Hz, 1 H), 6.22 (d, J = 7.6 Hz, 1 H), 1.61 (s, 6 H), 1.16 (s, 9 H), 0.99−0.90 (m, 9 H), 0.68−0.55 (m, 6 H); one exchangeable proton was not observed. MS m/z 661.0 $[M + H]^+$ (661.2 calcd for $C_{32}H_{43}ClFN_4O_2S_2Si^+$).

Hydrogen chloride (11 mL of a 4.0 M solution with 1,4-dioxane, 44 mmol) was added to a solution of **51** (2.9 g, 4.4 mmol) and methanol (44 mL) at room temperature. After 20 min, the reaction mixture was concentrated under reduced pressure, the residue was partitioned between ethyl acetate and saturated aqueous sodium bicarbonate, the layers were separated, the organic material was washed sequentially with saturated aqueous sodium bicarbonate and brine, dried (sodium sulfate), filtered, and the filtrate was concentrated under reduced pressure to give 2-(2-(2-((*R*)-amino(2-amino-5-chloro-3-fluoro-4-pyridinyl)methyl)-1-benzothiophen-7-yl)-4-pyridinyl)-2-propanol (1.9 g, quant yield) as a pale yellow solid. The material was used in the next step of the synthesis without purification.

4-Dimethylaminopyridine (0.052 g, 0.43 mmol) was added to a solution of 2-(2-(2-((*R*)-amino(2-amino-5-chloro-3-fluoro-4-pyridinyl)methyl)-1-benzothiophen-7-yl)-4-pyridinyl)-2-propanol (1.9 g, 4.3 mmol), *N*,*N*-dimethylformamide (4.3 mL), diisopropylethylamine (2.2 mL, 13 mmol), and cyclopropanesulfonyl chloride (0.66 mL, 6.4 mmol) at room temperature. After 21 h, saturated aqueous sodium bicarbonate and ethyl acetate were added, the mixture was stirred for 20 min, partitioned between more ethyl acetate and saturated aqueous sodium bicarbonate, the layers were separated, the organic material was washed sequentially with saturated aqueous sodium bicarbonate (4×) and brine (2×), dried (sodium sulfate), filtered, and the filtrate was concentrated under reduced pressure. The residue was subjected to flash chromatography on silica gel (49:1 dichloromethane−methanol) to give *N*-((*R*)-(2-amino-5-chloro-3-fluoro-4-pyridinyl)(7-(4-(1-hydroxy-1-methylethyl)-2-pyridinyl)-1-benzothiophen-2-yl)methyl)cyclopropanesulfonamide (**32**; 2.0 g, 83% yield) as an off-white solid. $[\alpha]^{30}_D$ +27.6° (c 1.42, $CHCl_3$). ^{1}H NMR (400 MHz, DMSO-d_6) δ 8.70 (d, J = 5.1 Hz, 1 H), 8.67 (d, J = 8.8 Hz, 1 H), 8.22 (s, 1 H), 8.11 (d, J = 7.2 Hz, 1 H), 7.92 (s, 1 H), 7.90 (d, J = 7.4 Hz, 1 H), 7.53 (t, J = 7.6 Hz, 1 H), 7.48 (dd, J = 1.5, 5.2 Hz, 1 H), 7.36−7.29 (m, 1 H), 6.56 (s, 2 H), 6.31 (d, J = 8.8 Hz, 1 H), 5.35 (s, 1 H), 2.48−2.39 (m, 1 H), 1.50 (s, 6 H), 1.02−0.76 (m, 4 H). ^{13}C NMR (125 MHz, DMSO-d_6) δ 160.3, 154.4, 149.2 (d, J = 12.7 Hz), 147.9, 145.1, 143.7 (d, J = 260.7 Hz), 141.8 (br d, J = 6.4 Hz), 140.5, 136.1, 132.4, 132.4 (br d, J = 10.0 Hz), 124.8, 124.7, 122.5, 121.3, 118.9, 116.5, 115.0, 70.5, 50.9, 31.1, 31.1, 30.7, 5.0, 5.0. HRMS m/z 547.1034 $[M + H]^+$ (547.1035 calcd for $C_{25}H_{25}ClFN_4O_3S_2^+$).

■ ASSOCIATED CONTENT

Supporting Information

The Supporting Information is available free of charge on the ACS Publications website at DOI: 10.1021/acs.jmedchem.5b01367.

Experimental procedures and characterization data for compounds **7**, **9**, **11**, **13**−**24**, and **26**−**30**,[38] absolute stereochemistry determinations for compound **31** and intermediate **38**, energetic parameters from the quantum mechanical analysis of the model systems in Figure 4, as well as statistical analyses of compound activities in key biological assays (PDF)

Molecular formula strings (CSV)

Accession Codes

Atomic coordinates for the X-ray crystal structures of compounds **6**, **12**, **26**, and **32** bound to hGKRP (2.2, 2.4, 2.6, and 2.2 Å resolution for **6**, **12**, **26**, and **32**, respectively) have been deposited in the RCSB (PDB codes 4PX2, 4PX3, 4PXS, and 4PX5 for **6**, **12**, **26**, and **32**, respectively).

■ AUTHOR INFORMATION

Corresponding Authors

*L.D.P.: phone, +1-781-609-6868; e-mail, lewis.pennington@alkermes.com.

*M.D.B.: phone, +1 805-447-3446; e-mail, mbartber@amgen.com.

Present Address

#L.D.P.: Alkermes, 852 Winter Street, Waltham, MA 02451.

Notes

The authors declare the following competing financial interest(s): All authors are current or former employees of Amgen.

■ ACKNOWLEDGMENTS

We thank Christopher Wilde (Molecular Structure and Characterization, Amgen) and Iain Campuzano (Molecular Structure and Characterization, Amgen) for confirmation of the structure assignments of **12**, **25**, **31**, and **32** using NMR and HRMS methods, respectively; Kyung-Hyun Gahm, Samuel Thomas, Wesley Barnhart, and Zheng Hua (Molecular Structure and Characterization, Amgen) for conducting compound separations by chiral SFC; Robert Kurzeja (Protein

DOI: 10.1021/acs.jmedchem.5b01367
J. Med. Chem. XXXX, XXX, XXX−XXX

Technologies, Amgen) for providing purified proteins; Robert Wahl and Kui Chen (Molecular Structure and Characterization, Amgen) for developing biochemical assays; David Cronk, Andrew Southan, Scott Pollack, and Kevin Nash (Compound Libraries and Assay Development and Screening, BioFocus) for executing the HTS campaign; Ramesh Senaiar and co-workers (Medicinal Chemistry, Aurigene) for preparing synthetic intermediates; and Scott Simonet and Murielle Véniant (Metabolic Disorders Research, Amgen), Dean Hickman (Pharmacokinetics and Metabolism, Amgen), and Philip Tagari (Therapeutic Discovery, Amgen) for endorsing this research. The Advanced Light Source for X-ray analyses was supported by the U.S. Department of Energy under Contract DE-AC02-05CH11231. All live animal studies were conducted in an AAALAC-accredited facility, and husbandry procedures met all of the recommendations of the Guide for the Care and Use of Laboratory Animals. All work using research animals was conducted under Institutional Animal Care and Use Committee (IACUC) approved protocols.

■ ABBREVIATIONS USED

T2DM, type II diabetes mellitus; GK, glucokinase; GKRP, glucokinase regulatory protein; G6P, glucose 6-phosphate; TL, translocation; RLM, rat liver microsome; CL_{int}, intrinsic clearance; cLogP, calculated log *P* (logarithm of the octanol/water partition coefficient) using the Daylight Chemical Information Systems algorithm; ACDLogP, calculated log *P* using the Advanced Chemistry Development (ACD/Labs) algorithm; $ACDLogD_{7.4}$, calculated log *D* using the Advanced Chemistry Development (ACD/Labs) algorithm; K_d, dissociation constant; P_{app}, apparent permeability; HPMC, hydroxypropyl methylcellulose; PPB, plasma protein binding; CL, clearance of compound from plasma; V_{dss}, volume of distribution at steady state; $t_{1/2}$, half-life of compound in plasma; C_{max}, maximum compound concentration in plasma; t_{max}, time at which maximum compound concentration in plasma was achieved; AUC, area under the plasma concentration−time curve; *F*, bioavailability; POC, percent-of-control; NBO, natural bond orbital; B3LYP, Becke, three-parameter, Lee−Yang−Parr hybrid density functional

■ REFERENCES

(1) International Diabetes Federation. IDF Diabetes Atlas. http://www.idf.org/ (accessed May 26, 2015).

(2) (a) Ettaro, L.; Songer, T. J.; Zhang, P.; Engelgau, M. M. Cost-of-illness studies in diabetes mellitus. *PharmacoEconomics* **2004**, *22*, 149−164. (b) Seuring, T.; Archangelidi, O.; Suhrcke, M. The economic costs of type 2 diabetes: a global systematic review. *PharmacoEconomics* **2015**, *33*, 811−831.

(3) Verspohl, E. J. Novel pharmacological approaches to the treatment of type 2 diabetes. *Pharmacol. Rev.* **2012**, *64*, 188−237.

(4) (a) Agius, L. Glucokinase and molecular aspects of liver glycogen metabolism. *Biochem. J.* **2008**, *414*, 1−18. (b) Matschinsky, F. M. Glucokinase as glucose sensor and metabolic signal generator in pancreatic β-cells and hepatocytes. *Diabetes* **1990**, *39*, 647−652.

(5) Matschinsky, F. M.; Glaser, B.; Magnuson, M. A. Pancreatic beta-cell glucokinase: closing the gap between theoretical concepts and experimental realities. *Diabetes* **1998**, *47*, 307−315.

(6) (a) Sarabu, R.; Grimsby, J. Targeting glucokinase activation for the treatment of type 2 diabetes—a status review. *Curr. Opin. Drug Discovery Dev.* **2005**, *8*, 631−637. (b) Meininger, G. E.; Scott, R.; Alba, M.; Shentu, Y.; Luo, E.; Amin, H.; Davies, M. J.; Kaufman, K. D.; Goldstein, B. J. Effects of MK-0941, a novel glucokinase activator, on glycemic control in insulin-treated patients with type 2 diabetes. *Diabetes Care* **2011**, *34*, 2560−2566. (c) Matschinsky, F. M.; Zelent, B.; Doliba, N.; Li, C.; Vanderkooi, J. M.; Naji, A.; Sarabu, R.; Grimsby, J. Glucokinase activators for diabetes therapy (May 2010 status report). *Diabetes Care* **2011**, *34* (Suppl. 2), S236−S243.

(7) (a) Rees, M. G.; Gloyn, A. L. Small molecular glucokinase activators: has another new anti-diabetic therapeutic lost favor? *Br. J. Pharmacol.* **2013**, *168*, 335−338. (b) Matschinsky, F. M. GKAs for diabetes therapy: why no clinically useful drug after two decades of trying? *Trends Pharmacol. Sci.* **2013**, *34*, 90−99.

(8) Filipski, K. J.; Pfefferkorn, J. A. A patent review of glucokinase activators and disruptors of the glucokinase − glucokinase regulatory protein interaction: 2011−2014. *Expert Opin. Ther. Pat.* **2014**, *24*, 875−891.

(9) Anderka, O.; Boyken, J.; Aschenbach, U.; Batzer, A.; Boscheinen, O.; Schmoll, D. Biophysical characterization of the interaction between hepatic glucokinase and its regulatory protein: impact of physiological and pharmacological effectors. *J. Biol. Chem.* **2008**, *283*, 31333−31340.

(10) Vandercammen, A.; Van Schaftingen, E. The mechanism by which rat liver glucokinase is inhibited by the regulatory protein. *Eur. J. Biochem.* **1990**, *191*, 483−489.

(11) Lloyd, D. J.; St. Jean, D. J., Jr.; Kurzeja, R. J. M.; Wahl, R. C.; Michelsen, K.; Cupples, R.; Chen, M.; Wu, J.; Sivits, G.; Helmering, J.; Ashton, K. S.; Pennington, L. D.; Fotsch, C. H.; Vazir, M.; Chen, K.; Chmait, S.; Zhang, J.; Liu, L.; Norman, M. H.; Andrews, K. A.; Bartberger, M. D.; Van, G.; Galbreath, E. J.; Vonderfecht, S. L.; Wang, M.; Jordan, S. R.; Veniant, M. M.; Hale, C. Antidiabetic effects of glucokinase regulatory protein small-molecule disruptors. *Nature* **2013**, *504*, 437−440.

(12) Ashton, K. S.; Andrews, K. L.; Bryan, M. C.; Chen, J.; Chen, K.; Chen, M.; Chmait, S.; Croghan, M.; Cupples, R.; Fotsch, C.; Helmering, J.; Jordan, S. R.; Kurzeja, R. J. M.; Michelsen, K.; Pennington, L. D.; Poon, S. F.; Sivits, G.; Van, G.; Vonderfecht, S. L.; Wahl, R. C.; Zhang, J.; Lloyd, D. J.; Hale, C.; St. Jean, D. J., Jr. Small molecule disruptors of the glucokinase−glucokinase regulatory protein interaction: 1. Discovery of a novel tool compound for in vivo proof-of-concept. *J. Med. Chem.* **2014**, *57*, 309−324.

(13) St. Jean, D. J., Jr.; Ashton, K. S.; Bartberger, M. D.; Chen, J.; Chmait, S.; Cupples, R.; Galbreath, E.; Helmering, J.; Hong, F.-T.; Jordan, S. R.; Liu, L.; Kunz, R. K.; Michelsen, K.; Nishimura, N.; Pennington, L. D.; Poon, S. F.; Reid, D.; Sivits, G.; Stec, M. M.; Tadesse, S.; Tamayo, N.; Van, G.; Yang, K.; Zhang, J.; Norman, M. H.; Fotsch, C.; Lloyd, D. J.; Hale, C. Small molecule disruptors of the glucokinase−glucokinase regulatory protein interaction: 2. Leveraging structure-based drug design to identify analogs with improved pharmacokinetic profiles. *J. Med. Chem.* **2014**, *57*, 325−338.

(14) Structurally related variations of the sulfonylpiperazine scaffold present in **3**−**5** have been subsequently reported by our laboratories: (a) Nishimura, N.; Norman, M. H.; Liu, L.; Yang, K. C.; Ashton, K. S.; Bartberger, M. D.; Chmait, S.; Chen, J.; Cupples, R.; Fotsch, C.; Helmering, J.; Jordan, S. R.; Kunz, R. K.; Pennington, L. D.; Poon, S. F.; Siegmund, A.; Sivits, G.; Lloyd, D. J.; Hale, C.; St. Jean, D. J., Jr. Small molecule disruptors of the glucokinase−glucokinase regulatory protein interaction: 3. Structure−activity relationships within the aryl carbinol region of the *N*-arylsulfonamido-*N*′-aryl-piperazine series. *J. Med. Chem.* **2014**, *57*, 3094−3116. (b) Hong, F.-T.; Norman, M. H.; Ashton, K. S.; Bartberger, M. D.; Chen, J.; Chmait, S.; Cupples, R.; Fotsch, C.; Jordan, S. R.; Lloyd, D. J.; Sivits, G.; Tadesse, S.; Hale, C.; St. Jean, D. J., Jr. Small molecule disruptors of the glucokinase−glucokinase regulatory protein interaction: 4. Exploration of a novel binding pocket. *J. Med. Chem.* **2014**, *57*, 5949−5964. (c) Tamayo, N. A.; Norman, M. H.; Bartberger, M. D.; Hong, F.-T.; Bo, Y.; Liu, L.; Nishimura, N.; Yang, K. C.; Tadesse, S.; Fotsch, C.; Chen, J.; Chmait, S.; Cupples, R.; Hale, C.; Jordan, S. R.; Lloyd, D. J.; Sivits, G.; St. Jean, D. J., Jr. Small molecule disruptors of the glucokinase−glucokinase regulatory protein interaction: 5. A novel aryl sulfone series, optimization through conformational analysis. *J. Med. Chem.* **2015**, *58*, 4462−4482.

(15) For the original design and execution of this GKRP HTS strategy, see the following: Chen, K.; Michelsen, K.; Kurzeja, R. J. M.; Han, J.; Vazir, M.; St. Jean, D. J., Jr.; Hale, C.; Wahl, R. C. Discovery of

DOI: 10.1021/acs.jmedchem.5b01367
J. Med. Chem. XXXX, XXX, XXX−XXX

small-molecule glucokinase regulatory protein modulators that restore glucokinase activity. *J. Biomol. Screening* **2014**, *19*, 1014−1023.
(16) The first HTS campaign of nearly 2 million compounds also resulted in only a single potent, selective, and structurally distinct hit **3**.
(17) For detailed descriptions of the surface plasmon resonance assay (Biacore) using human GK or human, rat, or mouse GKRP constructs, as well as the bead-based proximity assay (AlphaScreen) using human GK and GKRP constructs, see refs 11−14.
(18) (a) cLogP and PSA were calculated with the Daylight Suite, version 4.81, Daylight Chemical Information Systems, Inc. (b) ACDLogP and $ACDLogD_{7.4}$ were calculated with ACD 2012, Advanced Chemistry Development, Inc. (ACD/Labs).
(19) Very little protein backbone or side chain movement was found to occur upon the binding of **3** versus **6** with GKRP: the rmsd (both backbone and side chain atoms) of common residues within a 4.5 Å radius of either **3** or **6** is only ∼0.76 Å.
(20) Botta, M.; Corelli, F.; Gasparrini, F.; Messina, F.; Mugnaini, C. Chiral azole derivatives. 4. Enantiomers of bifonazole and related antifungal agents: synthesis, configuration assignment, and biological evaluation. *J. Org. Chem.* **2000**, *65*, 4736−4739 (see the Supporting Information for details).
(21) For detailed descriptions of this cell assay using mouse or rat primary hepatocytes, see refs 11−14.
(22) Johansson, M. P.; Olsen, J. Torsional barriers and equilibrium angle of biphenyl: reconciling theory with experiment. *J. Chem. Theory Comput.* **2008**, *4*, 1460−1471.
(23) For a recent comprehensive review, see the following: Beno, B. R.; Yeung, K.-S.; Bartberger, M. D.; Pennington, L. D.; Meanwell, N. A. A survey of the role of noncovalent sulfur interactions in drug design. *J. Med. Chem.* **2015**, *58*, 4383−4438.
(24) Yu, G. J.; Yoo, C. L.; Yang, B.; Lodewyk, M. W.; Meng, L.; El-Idreesy, T. T.; Fettinger, J. C.; Tantillo, D. J.; Verkman, A. S.; Kurth, M. J. Potent *s-cis*-locked bithiazole correctors of ΔF508 cystic fibrosis transmembrane conductance regulator cellular processing for cystic fibrosis therapy. *J. Med. Chem.* **2008**, *51*, 6044−6054.
(25) Lin, S.; Wrobleski, S. T.; Hynes, J., Jr.; Pitt, S.; Zhang, R.; Fan, Y.; Doweyko, A. M.; Kish, K. F.; Sack, J. S.; Malley, M. F.; Kiefer, S. E.; Newitt, J. A.; McKinnon, M.; Trzaskos, J.; Barrish, J. C.; Dodd, J. H.; Schieven, G. L.; Leftheris, K. Utilization of a nitrogen−sulfur nonbonding interaction in the design of new 2-aminothiazol-5-ylpyrimidines as p38α MAP kinase inhibitors. *Bioorg. Med. Chem. Lett.* **2010**, *20*, 5864−5868.
(26) All quantum mechanical calculations were performed within the Gaussian 09 program system: Frisch, M. J.; Trucks, G. W.; Schlegel, H. B.; Scuseria, G. E.; Robb, M. A.; Cheeseman, J. R.; Scalmani, G.; Barone, V.; Mennucci, B.; Petersson, G. A.; Nakatsuji, H.; Caricato, M.; Li, X.; Hratchian, H. P.; Izmaylov, A. F.; Bloino, J.; Zheng, G.; Sonnenberg, J. L.; Hada, M.; Ehara, M.; Toyota, K.; Fukuda, R.; Hasegawa, J.; Ishida, M.; Nakajima, T.; Honda, Y.; Kitao, O.; Nakai, H.; Vreven, T.; Montgomery, J. A., Jr.; Peralta, J. E.; Ogliaro, F.; Bearpark, M.; Heyd, J. J.; Brothers, E.; Kudin, K. N.; Staroverov, V. N.; Keith, T.; Kobayashi, R.; Normand, J.; Raghavachari, K.; Rendell, A.; Burant, J. C.; Iyengar, S. S.; Tomasi, J.; Cossi, M.; Rega, N.; Millam, J. M.; Klene, M.; Knox, J. E.; Cross, J. B.; Bakken, V.; Adamo, C.; Jaramillo, J.; Gomperts, R.; Stratmann, R. E.; Yazyev, O.; Austin, A. J.; Cammi, R.; Pomelli, C.; Ochterski, J. W.; Martin, R. L.; Morokuma, K.; Zakrzewski, V. G.; Voth, G. A.; Salvador, P.; Dannenberg, J. J.; Dapprich, S.; Daniels, A. D.; Farkas, O.; Foresman, J. B.; Ortiz, J. V.; Cioslowski, J.; Fox, D. J. *Gaussian 09*, revision D.01; Gaussian, Inc.: Wallingford, CT, U.S., 2009.
(27) NBO 6.0. Glendening, E. D.; Badenhoop, J. K.; Reed, A. E.; Carpenter, J. E.; Bohmann, J. A.; Morales, C. M.; Landis, C. R.; Weinhold, F. Theoretical Chemistry Institute, University of Wisconsin, Madison, 2013.
(28) Weinhold, F.; Landis, C. R. Natural bond orbitals and extensions of localized bonding concepts. *Chem. Educ. Res. Pract.* **2001**, *2*, 91−104.
(29) For a recent review, see the following: Gillis, E. P.; Eastman, K. J.; Hill, M. D.; Donnelly, D. J.; Meanwell, N. A. Applications of fluorine in medicinal chemistry. *J. Med. Chem.* **2015**, *58*, 8315−8359.
(30) St. Jean, D. J., Jr.; Fotsch, C. Mitigating heterocycle metabolism in drug discovery. *J. Med. Chem.* **2012**, *55*, 6002−6020.
(31) For detailed descriptions of this GK translocation assay using Sprague−Dawley rats, see refs 11−14.
(32) Interestingly, the total plasma concentration of **31** (2.9 μM) coinciding with statistically significant GK translocation (TL) at the 6 h time point for the 10 mg/kg dose translates into an unbound plasma concentration (0.029 μM; PPB = 99%; Table 5) that is well below the cellular potency of **31** (rGK TL EC_{50} = 0.14 for **31**).[21,31] Similarly, the total plasma concentration of **31** or **32** (∼0.20 μM) coinciding with statistically significant GK translocation (TL) at the 24 h time point for the 10 mg/kg dose translates into an unbound plasma concentration (∼0.0020 μM; PPB = 99%; Table 5) that is even further below the cellular potency of **31** or **32** (rGK TL EC_{50} = 0.037 μM for **32**). It should be noted that for in vivo experiments GK TL was measured using an immunohistochemistry readout with visual scoring, and for in vitro experiments GK TL was measured using a differential fluorescence intensity readout with confocal microscopy detection.[21,31] One explanation for this exposure−effect disconnect may be that compounds **31** and **32** achieve higher concentrations in liver tissue than in plasma.
(33) For detailed descriptions of this blood glucose assay using db/db mice, see refs 11−14.
(34) Statistically significant blood glucose lowering was not achieved at the 3 h time point for the 100 mg/kg dose of **31** but was achieved at this time point for the 10 mg/kg dose of **31**; this discrepancy is attributed to the variability in the measured blood glucose levels for the 100 mg/kg dose of **31** at the 3 h time point.
(35) The whole-blood concentration of **31** (19 μM) coinciding with statistically significant blood glucose lowering at the 6 h time point for the 100 mg/kg dose is ∼40-fold higher than the cellular potency of **31** (mGK TL EC_{50} = 0.48 μM).[33] It should be noted that **31** is likely highly protein bound in mouse (rat PPB = 99%; Table 5).
(36) Although the variability in the measured blood glucose levels confounds clear interpretation, it was also encouraging to observe statistically significant blood glucose lowering at the 3 and 6 h time points for the 10 and 30 mg/kg doses of **32**, respectively.
(37) The whole-blood concentration of **32** (21−25 μM) coinciding with statistically significant blood glucose lowering at the 3 and 6 h time points for the 100 mg/kg dose is ∼320- to 380-fold higher than the cellular potency of **32** (mGK TL EC_{50} = 0.066 μM).[33] It should be noted that **32** is likely highly protein bound in mouse (rat PPB = 99%; Table 5).
(38) For the initial disclosure of the chemical synthesis of these compounds, see the following: (a) Bartberger, M. D.; Croghan, M. D.; Fotsch, C. H.; Norman, M. H.; Pennington, L. D.; Reichelt, A.; St. Jean, D. J., Jr.; Tegley, C. M. Benzodioxepine and benzodioxine compounds that interact with glucokinase regulatory protein for the treatment of diabetes. WIPO/PCT Pat. Appl. WO 2012138776 A1, 2012. (b) Ashton, K.; Bartberger, M. D.; Bourbeau, M. P.; Croghan, M. D.; Fotsch, C. H.; Hungate, R. W.; Kong, K.; Nishimura, N.; Norman, M. H.; Pennington, L. D.; Reichelt, A.; Siegmund, A. C.; Tadesse, S.; St. Jean, D. J., Jr.; Yang, K. C.; Yao, G. Benzothiophene sulfonamides and other compounds that interact with glucokinase regulatory protein. WIPO/PCT Pat. Appl. WO 2013173382 A1, 2013.
(39) For a comprehensive review of the synthetic and stereochemical aspects of *tert*-butanesulfinylimine chemistry, see the following: Robak, M. T.; Herbage, M. A.; Ellman, J. A. Synthesis and applications of *tert*-butanesulfinamide. *Chem. Rev.* **2010**, *110*, 3600−3740.
(40) Assignments of the absolute configuration of **38** and its antipode were determined by comparison of their computed and measured vibrational circular dichroism (VCD) spectra (Stephens, P. J.; Devlin, F. J.; Pan, J.-J. *Chirality* **2008**, *20*, 643−663) and optical rotations; see the Supporting Information for details.
(41) Akay, S.; Yang, W.; Wang, J.; Lin, L.; Wang, B. Synthesis and evaluation of dual wavelength fluorescent benzo[b]thiophene boronic

DOI: 10.1021/acs.jmedchem.5b01367
J. Med. Chem. XXXX, XXX, XXX−XXX

acid derivatives for sugar sensing. *Chem. Biol. Drug Des.* **2007**, *70*, 279−289.
(42) Assignments of the absolute configuration of **31** and its antipode were determined by comparison of their computed and measured optical rotations; see the Supporting Information for details.
(43) Schlosser, M.; Bobbio, C. Creating structural manifolds from a common precursor: basicity gradient-driven isomerization of halopyridines. *Eur. J. Org. Chem.* **2002**, 4174−4180.
(44) For the experimental details of key biological assays, see refs 11−14.

DOI: 10.1021/acs.jmedchem.5b01367
J. Med. Chem. XXXX, XXX, XXX−XXX